Circulation Patterns and Associated Rainfall Over South Tropical South America: GCMs Evaluation During the Dry-To-Wet Transition Season

M. Olmo, J.-c. Espinoza, M. Bettolli, J. P. Sierra, C. Junquas, P. Arias, Vincent Moron, R. Balmaceda-Huarte

JGR Atmospheres

RESEARCH ARTICLE
10.1029/2022JD036468

Circulation Patterns and Associated Rainfall Over South Tropical South America: GCMs Evaluation During the Dry-To-Wet Transition Season

M. E. Olmo[1,2,3], J.-C. Espinoza[4], M. L. Bettolli[1,2,3], J. P. Sierra[4], C. Junquas[4], P. A. Arias[5], V. Moron[6,7], and R. Balmaceda-Huarte[1,2,3]

[1]Department of Atmospheric and Ocean Sciences, Faculty of Exact and Natural Sciences, University of Buenos Aires (DCAO-FCEN-UBA), Buenos Aires, Argentina, [2]National Council of Scientific and Technical Research (CONICET), Buenos Aires, Argentina, [3]Institut Franco-Argentin d'Estudes sur le Climat et ses Impacts, Unité Mixte Internationale (UMI-IFAECI/CNRS-CONICET-UBA-IRD), Buenos Aires, Argentina, [4]Univ. Grenoble Alpes, IRD, CNRS, Grenoble INP, IGE, Grenoble, France, [5]Grupo de Ingeniería y Gestión Ambiental, Escuela Ambiental, Facultad de Ingeniería, Universidad de Antioquia, Medellín, Colombia, [6]Aix-Marseille University, CNRS, IRD, INRAE, Collège de France CEREGE, Aix-en-Provence, France, [7]Lamont-Doherty Earth Observatory, International Research Institute for Climate and Society, Columbia University, Palisades, NY, USA

Abstract The representation of the South American Monsoon System (SAMS) by general circulation models (GCMs) is of key relevance for a better understanding of the physical rationale behind the recent climate changes over South Tropical South America (STSA) and their expected changes in a global warming scenario. During the last four decades, STSA experienced a lengthening of the dry season associated with diverse forcings. In this work, a set of 16 GCMs historical Coupled Model Intercomparison Project Phase 6 coupled simulations were evaluated during 1979–2014 in terms of how well they reproduced the atmospheric circulation over STSA through a circulation-patterns (CPs) approach. Nine CPs were first identified based on low-level winds from the ERA5 reanalysis. Focus was put on the representation of CPs during the dry-to-wet transition season (July-October). Model performance depended on the seasonal cycle and spatial structure of the CPs. GCMs adequately reproduced the different CPs, with lower skills in the transition seasons. GCMs tended to go from dry to wet conditions too quickly, evidencing deficiencies in the representation of the SAMS onset, related to a poor representation of the southerly wind intrusions to STSA and the variability of the South American low-level jet. Some GCMs were able to associate the occurrence of anomalous dry and wet years with specific CPs, suggesting well-represented physical mechanisms controlling precipitation variability. This study could identify a few GCMs that adequately simulated the CPs in STSA (among them, CESM2, CMCC-CM2-HR4 and MPI-ESM1-2-HR), which is relevant for driving high-resolution models and the analysis of future projections.

Key Points:

- Some general circulation models (GCMs) adequately represented both the seasonal cycle and spatial structure of circulation patterns
- GCMs often struggled in representing the monsoon initiation and the variability of the South American low-level jet
- GCMs tended to go from dry to wet conditions too quickly

Supporting Information:

Supporting Information may be found in the online version of this article.

Correspondence to:

M. E. Olmo,
molmo@at.fcen.uba.ar

Citation:

Olmo, M. E., Espinoza, J.-C., Bettolli, M. L., Sierra, J. P., Junquas, C., Arias, P. A., et al. (2022). Circulation patterns and associated rainfall over south tropical South America: GCMs evaluation during the dry-to-wet transition season. *Journal of Geophysical Research: Atmospheres*, *127*, e2022JD036468. https://doi.org/10.1029/2022JD036468

Received 10 JAN 2022
Accepted 26 MAY 2022

Author Contributions:

Conceptualization: M. E. Olmo, J.-C. Espinoza, J. P. Sierra, C. Junquas, P. A. Arias, V. Moron
Data curation: M. E. Olmo, J. P. Sierra
Formal analysis: M. E. Olmo, J.-C. Espinoza, J. P. Sierra, C. Junquas, P. A. Arias, V. Moron, R. Balmaceda-Huarte
Funding acquisition: J.-C. Espinoza
Investigation: M. E. Olmo, J.-C. Espinoza, J. P. Sierra, C. Junquas, P. A. Arias, V. Moron, R. Balmaceda-Huarte
Methodology: M. E. Olmo, J.-C. Espinoza, C. Junquas, P. A. Arias, V. Moron
Project Administration: J.-C. Espinoza
Resources: J.-C. Espinoza
Software: M. E. Olmo, J. P. Sierra
Supervision: J.-C. Espinoza

1. Introduction

South Tropical South America (STSA), extended approximately between 10°N–30°S and 90°W–30°W, is a wide region where diverse interactions among biomass, land surface processes and atmospheric convection take place. These interactions modulate the local and regional climate and directly impact on the socio-environmental activities (Fu et al., 2013; Reis et al., 2018; Zhang et al., 2015). STSA hosts the Amazonia - the world's largest rainforest and one of the major sources of evapotranspiration - playing a critical role in the global balances of energy, water, moisture and carbon (Gatti et al., 2021; Llopart et al., 2020). The region presents unique biodiversity and geographical patterns, mainly due to the interaction of the Amazonia and the Andes mountain range, which have deep implications in the atmospheric dynamics, moisture transport and river discharge not only throughout STSA but also in remote regions of the continent (Arias, Garreaud, et al., 2021; Espinoza et al., 2020; Sierra et al., 2021).

Precipitation (PP) over STSA presents a marked spatio-temporal variability, strongly controlled by the South American Monsoon System (SAMS), with rainfall maxima during its active phase during the austral summer (Marengo et al., 2012; Vera et al., 2006). The monsoonal circulation - which develops in response to seasonal changes in thermal land-sea contrasts - is connected to different documented atmospheric features, including a NW-SE band of convergence and convective activity over the southeast of South America and the adjacent South Atlantic ocean known as the South Atlantic Convergence Zone (SACZ), an anticyclonic center located

Validation: M. E. Olmo, C. Junquas, P. A. Arias, V. Moron, R. Balmaceda-Huarte
Visualization: M. E. Olmo, J.-C. Espinoza, J. P. Sierra, R. Balmaceda-Huarte
Writing – original draft: M. E. Olmo, J.-C. Espinoza, J. P. Sierra, C. Junquas, P. A. Arias, V. Moron, R. Balmaceda-Huarte

in the upper-troposphere over Bolivia (Bolivian high) and the presence of the low-level jet of South America (SALLJ) east of the Andes (Carvalho et al., 2004; Carvalho & Silva-Dias, 2021; da Anunciação et al., 2014; Gan et al., 2004; Garreaud, 2009; Grimm et al., 2020; Montini et al., 2019; Nogués-Paegle & Mo, 1997; Wang & Fu, 2002).

During the recent decades, STSA has experienced an increase in dry conditions over southern Amazonia – around 5°–15°S and 70°–50°W – during the dry-to-wet transition season (approximately from July to October) and a lengthening of the dry season associated with a delayed SAMS onset (Arias et al., 2015; Correa et al., 2021; Debortoli et al., 2015; Espinoza et al., 2019; Fu et al., 2013; Giráldez et al., 2020; Pascale et al., 2019). The most recent climate report of the Intergovernmental Panel on Climate Change (IPCC) indicates high confidence on a delayed onset of the SAMS, which is influenced by anthropogenic forcings such as land-use and deforestation changes, that induce modifications in the STSA hydrological cycle and atmospheric circulation (Alves et al., 2017; Caballero et al., 2022; Costa & Pires, 2010; Marengo et al., 2018; Ruiz-Vasquez et al., 2020; Sierra et al., 2021; Silva et al., 2020; Wongchuig et al., 2021; Zilli & Carvalho, 2021). All of these topics are currently central issues within the scientific community since the modification of the surface-atmosphere feedbacks endangers biodiversity and human activities (Bombardi et al., 2019; Gatti et al., 2021; Staal et al., 2018).

Classifications of atmospheric circulation patterns (CPs) are useful tools for spatio-temporal climate variability studies and model evaluation. An extensive body of literature around the world has followed different weather-typing approaches for these purposes (Cahynová & Huth, 2016; Fleig et al., 2015; Moron et al., 2016; Schuenemann & Cassano, 2009; among others) and could identify the links between large-scale and regional-to-local scale processes, which can also help to improve the statistical modeling of surface variables such as temperature and PP (D'onofrio et al., 2010; Moron et al., 2008; Olmo & Bettolli, 2021b; San Martin et al., 2017). Over different portions of STSA, diverse studies considered observational data to characterize the synoptic environment and its links with different surface processes and climate hazards such as droughts, heatwaves and heavy rainfall events (da Anunciação et al., 2014; Espinoza et al., 2013, 2012; Figueroa et al., 2020; Loikith et al., 2019; Olmo & Bettolli, 2021a; Olmo et al., 2020; Paccini et al., 2018). More recently, Espinoza et al. (2021) assessed the evaluation of low-level CPs all year along over STSA during the recent period. The authors associated these CPs with different PP patterns and connected the previously mentioned lengthening of the dry season and delay of the SAMS onset with specific atmospheric configurations. In particular, they found an increasing frequency of a CP characterized by enhanced SALLJ and atmospheric subsidence over STSA and a decreasing frequency of another CP distinguished by southerly cold-air incursions and anomalous convective activity over STSA. This highlighted the convenience of describing the SAMS variability through this approach, given that wind circulation is frequently better modeled than surface variables with more complex spatial features (e.g., PP, evapotranspiration).

The use of general circulation models (GCMs) can provide essential tools for a better understanding of the physical mechanisms behind the recent and future climate changes over STSA, which can arise from natural variability or in response to changes in radiative forcing. In this line, the Coupled Model Intercomparison Project Phase 6 (CMIP6) experiment produces global coupled climate model outputs for the historical record (up to 2014) and for different projected scenarios for the 21st century (Eyring et al., 2016). The evaluation of the historical simulations allows us to assess model performance during the present climate, which is necessary to properly interpret the GCMs future projections. In particular, GCMs from CMIP6 and previous Coupled Model Intercomparison Project Phase (CMIP) experiments exhibited systematic errors in PP magnitudes over STSA, such as an underestimation over tropical South America and overestimation in the Andes and La Plata basin (Almazroui et al., 2021; Arias, Ortega, et al., 2021; Díaz et al., 2021; Gulizia & Camilloni, 2015; Ortega et al., 2021; Pabón-Caicedo et al., 2020; Sierra et al., 2015; Yin et al., 2013). In terms of long-term variability, GCMs depicted general drying trends during the historical period, especially over most of Amazonia, which are expected to intensify in the future (Almazroui et al., 2021; Boisier et al., 2015; Fu et al., 2013; Reboita et al., 2021; Sena & Magnusdottir, 2020; Teodoro et al., 2021; Thaler et al., 2021; Wainwright et al., 2021). Even more, according to Parsons (2020), the new generation of GCMs showed major agreement that most of the Amazonia will receive less PP in the future, with particularly strong agreement in eastern and southern Amazonia.

The representation of atmospheric circulation types by GCMs has been subject of study in other regions of the world (Bettolli & Penalba, 2014; Fernández-Granja et al., 2021; Gibson et al., 2016; Pinto et al., 2018; Stryhal & Huth, 2018), showing that although the GCMs are generally able to capture the key synoptic conditions of the different regions, they still exhibit significant biases in the representation of the CPs. This topic arises as an

interesting path to address model evaluation in light of the GCMs limitations in PP outputs as mentioned above. Notwithstanding, the GCMs performance on the CPs variability over STSA has not been explored yet.

Besides, the analysis of the CPs considering GCMs outputs could potentially help in the design of high-resolution modeling experiments over the region, which can provide a greater insight on the climate system response to the different documented changes over STSA, such as land-use perturbations. These limited-area models are nested with large-scale atmospheric variables as lateral boundary conditions – usually taken from GCMs – and provide a sophisticated representation of the physical processes (Ambrizzi et al., 2018; Solman, 2013). However, the skill of these regional simulations and their improvement compared to the driving GCM may be insufficient when large errors are present in the driving data (Fernández-Granja et al., 2021; Maraun et al., 2021). Consequently, the understanding of the main errors of the GCMs is especially relevant for well-founded policy making and adaptation decisions and impact on the projected signals.

All the described above remarks the complexity and importance of studying the diverse climate processes over STSA to get a full picture of the past and future changes in a context of global warming. Thereby, the aim of the present work is to perform a process-based assessment of a set of CMIP6 historical GCMs in simulating the atmospheric circulation and its associated rainfall over STSA as a follow-on study from Espinoza et al. (2021) using their weather-typing approach. Focus will be put on the spatio-temporal variability of CPs and, particularly, on the representation of the dry-to-wet (July-October) transition season. This paper is organized as follows: Section 2 presents the data and methodology used in this study, the main results are detailed and analyzed in Section 3 and the summary and final remarks are given in Section 4.

2. Data and Methodology

2.1. Reference Datasets

2.1.1. Atmospheric Data

The atmospheric circulation was described using daily zonal and meridional wind over STSA – between 10°N–30°S and 90°W–30°W – during the 1979–2014 period, from the European Centre for Medium-Range Weather Forecast (ECMWF) ERA5 reanalysis (Hersbach et al., 2020). Additionally, vertical velocity at different pressure levels between 1,000 and 100 hPa were also analyzed for each CP. The ERA5 data set is the state-of-the-art generation reanalysis from the ECMWF at ∼0.25° spatial resolution and the analysis is produced with a 1 hr time step. Data are available online (https://www.ecmwf.int/en/forecasts/datasets/reanalysis-datasets/era5). In this study, daily average data bilinearly interpolated into a 1.5° × 1.5° grid resolution were used to be compared with GCMs outputs.

2.1.2. Precipitation Data

The Climate Hazards Group Infrared Precipitation with Stations (CHIRPS) data set was considered for analyzing rainfall variability and its relationship with the CPs over STSA (Funk et al., 2014). This PP product is generated using satellite and rain gauge data and is available at ∼0.05° grid resolution at a daily scale from 1981 to the present. Previous studies evaluated and identified CHIRPS as a suitable data set over STSA as it adequately reproduced PP variability (Arias et al., 2020; Cavalcante et al., 2020; Olmo & Bettolli, 2021a; Segura et al., 2019; among others). In particular, Espinoza et al. (2019) studied wet and dry daily frequencies and related atmospheric features over southern Amazonia using this data set and obtained good correlations between CHIRPS and an independent data set of streamflow over the basin, indicating that CHIRPS is suitable for studying PP variability in the region. For this work, CHIRPS rainfall estimates were considered during the 1981–2014 period and re-gridded into a 1.5° × 1.5° spatial resolution to be compared with GCMs outputs. The CHIRPS V2.0 data are available online (https://data.chc.ucsb.edu/products/CHIRPS-2.0/global_daily/).

2.2. General Circulation Models

Historical coupled (atmosphere-ocean) simulations for the 1979–2014 period from the CMIP6 experiment (Eyring et al., 2016) were used in the evaluation of CPs over STSA. A set of 16 GCMs was used in this work (listed in Figure 1b), which has full availability for the variables of interest, including daily zonal and meridional winds, vertical velocity at six different levels – from 1,000 to 100 hPa – and accumulated PP. A more detailed

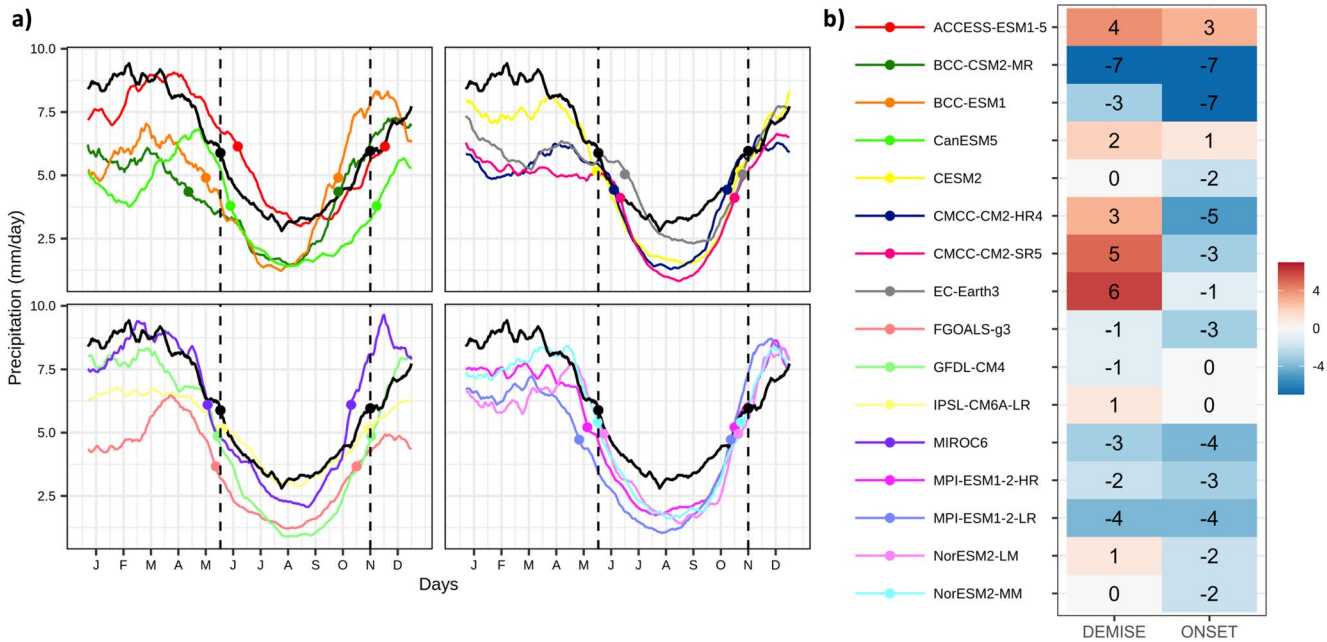

Figure 1. (a) Precipitation annual cycles over a part of the southern Amazonia (between 15°–5°S and 50°–70°W), expressed in mm/day and smoothed using a 5-day moving window. The black lines indicate the Climate Hazards Group Infrared Precipitation with Stations (CHIRPS) reference data set, and the colors indicate the different general circulation models (GCMs). The South American Monsoon System (SAMS) onset and demise in each data set are highlighted with dots; (b) Differences in the SAMS onset and demise between the CHIRPS reference data set and the GCMs quantified as the number of pentads.

description of the GCMs considered in this study is presented in Table S1 (see Supporting Information S1). Given the variety of GCMs spatial resolutions, all model outputs were interpolated into a common grid of 1.5° × 1.5° using bilinear interpolation, which was an intermediate grid resolution to intercompare them. Note that one model realization – r1i1p1f1 in all cases – was considered for the purpose of model evaluation and to limit the number of runs analyzed for computational efficiency. CMIP6 model outputs are available online through the Earth System Grid Federation (ESGF) CMIP data centres (https://esgf-node.llnl.gov/search/cmip6/).

2.3. Definition of Circulation Patterns

In order to evaluate whether the different GCMs are able to reproduce the observed atmospheric CPs or weather types over STSA as identified by Espinoza et al. (2021), a similar methodology is proposed here. In their study, Espinoza et al. (2021) identified and characterized nine intraseasonal CPs in tropical South America in agreement with previous studies (da Anunciação et al., 2014; Espinoza et al., 2012; Paccini et al., 2018). Daily CPs were constructed only based on zonal and meridional winds at 850 hPa. Standardized wind anomalies were calculated - using the long-term mean and standard deviation - and then clustered without any time filtering following a two-step procedure. First, the low-level wind anomalies were synthesized using the Empirical Orthogonal Function (EOF) technique conserving, at least, 75% of the total variance of the data. Second, a cluster analysis based on the subspace defined by the leading EOFs was performed using the k-means algorithm (Wilks, 2019). A more exhaustive description of this methodology is available in the Supporting Information S1. The clustering procedure was replicated for each GCM, so the simulated CPs could be compared to the ones identified in the ERA5 reanalysis. Model CPs were matched to the reference ERA5 CPs by comparing their respective centroids based on a minimum Euclidean distance criterion.

For the evaluation of model simulations in reproducing the CPs, different approaches are usually considered in terms of the input data (using raw variables or anomalies), projecting model daily fields into a reference classification (Bettolli & Penalba, 2014; Gibson et al., 2016) or including them in the clustering procedure (Pinto et al., 2018; Schuenemann & Cassano, 2009), as performed in this study. It is relevant to mention that a sensitivity analysis on the clustering methodology was performed by projecting each daily GCM field into the ERA5 centroids. The accuracy of model projection was quantified through the quantization error, which is estimated as

the average Euclidean distance between an input daily field and the reference centroids (Olmo & Bettolli, 2021a; Quagraine et al., 2020). The GCMs ranking obtained from this metric (see Table S2 in Supporting Information S1) agreed with the identification of the best GCMs as shown in the main results of the CPs discussed in the following sections. Although this projection procedure is commonly followed in the literature, by performing the clustering in each GCM independently one can give the GCMs the freedom to simulate their own dominant atmospheric patterns and then compare them to the ERA5 reference ones. Furthermore, because wind anomalies are calculated without any time filtering – thus, considering the seasonal cycle – it is expected that the GCMs should be able to simulate, at some point, these CPs without the need to be guided through a projection procedure (by informing the actual circulation structures). For these reasons, in this work we decided to perform the k-means clustering in each GCM, separately.

2.4. Evaluation Framework

The evaluation of the GCMs performance in reproducing the observed CPs as depicted by the ERA5 reanalysis was addressed on the basis of the seasonal cycle of the CPs, their spatial structure and associated rainfall. On one hand, focus was put on the models' ability to reproduce the seasonal distribution of CPs, with focus on the dry-to-wet transition season (July-October). This was quantified with an error metric that measures the absolute difference between the observed and modeled CP climatological daily frequencies as described in Equation 1, where D is the total number of days during the season (129 days) and $fERA5$ is the number of days assigned to a CP in the reanalysis-based classification, whereas $fGCM$ is analogous but for each GCM. This metric was calculated for the nine CPs, individually.

$$\text{Error}_{\text{CP}} = \frac{\sum_{i=1}^{D} |fERA5_{\text{CP}}i - fGCM_{\text{CP}}i|}{D} \quad (1)$$

As an example, if during the 1979–2014 period, 10 of the 36 July 1st days correspond to W2 (winter pattern 2) in ERA5, and 15 of the 36 July 1st correspond to W2 in a specific GCM, then the absolute difference is 5 days. This estimation is replicated for each day during the season and then all the 129 values are averaged, resulting in the Error value for W2 in that specific GCM.

On the other hand, the spatial patterns of the CPs were studied by constructing composites (mean fields) for each CP. Taylor diagrams were used for summarizing model performance, which quantify the degree of statistical similarity between the ERA5 reference data set and the different GCMs, reporting the Pearson correlation coefficient, the standard deviation and the centered root mean squared error (Taylor, 2001).

In addition, the link between large-scale atmospheric features and rainfall over STSA focused on the dry-to-wet transition season (July to October) at an interannual time-scale was explored. The relationship between the frequency of CPs and two rainfall indices - mean seasonal PP and dry-day (no accumulated PP) frequency (DDF) – was analyzed with the rank-based Kendall τ coefficient (Wilks, 2019). This coefficient was estimated for the detrended time-series (by removing, if any, the linear trend estimated from a linear regression analysis) using a confidence level of 95%.

3. Results

3.1. Precipitation Annual Cycle Over STSA

Given that the focus of this study is on the GCMs evaluation of the dominant atmospheric states and their associated rainfall over STSA, the PP annual cycle over part of southern Amazonia (between 15°–5°S and 50°–70°W) is presented in Figure 1a. Similar to previous works, the approximate onset and demise of the SAMS were identified when the PP values (expressed in pentads) reached the climatological annual mean rainfall (1979–2014), which was highlighted with dots in the cycles. Note, however, that this implies a more relaxed definition of the SAMS onset and demise than in previous studies considering observational datasets (Arias et al., 2015; Correa et al., 2021; Espinoza et al., 2021) to explore the GCMs performance. Differences in the SAMS onset and demise between the CHIRPS reference data set and the GCMs were quantified as the number of pentads in Figure 1b. Most of the GCMs were able to reproduce the shape of the south tropical PP annual cycle (e.g., ACCESS-ESM1-5 and IPSL-CM6A-LR), although they exhibited deficiencies in capturing the maximum rainfall values during the

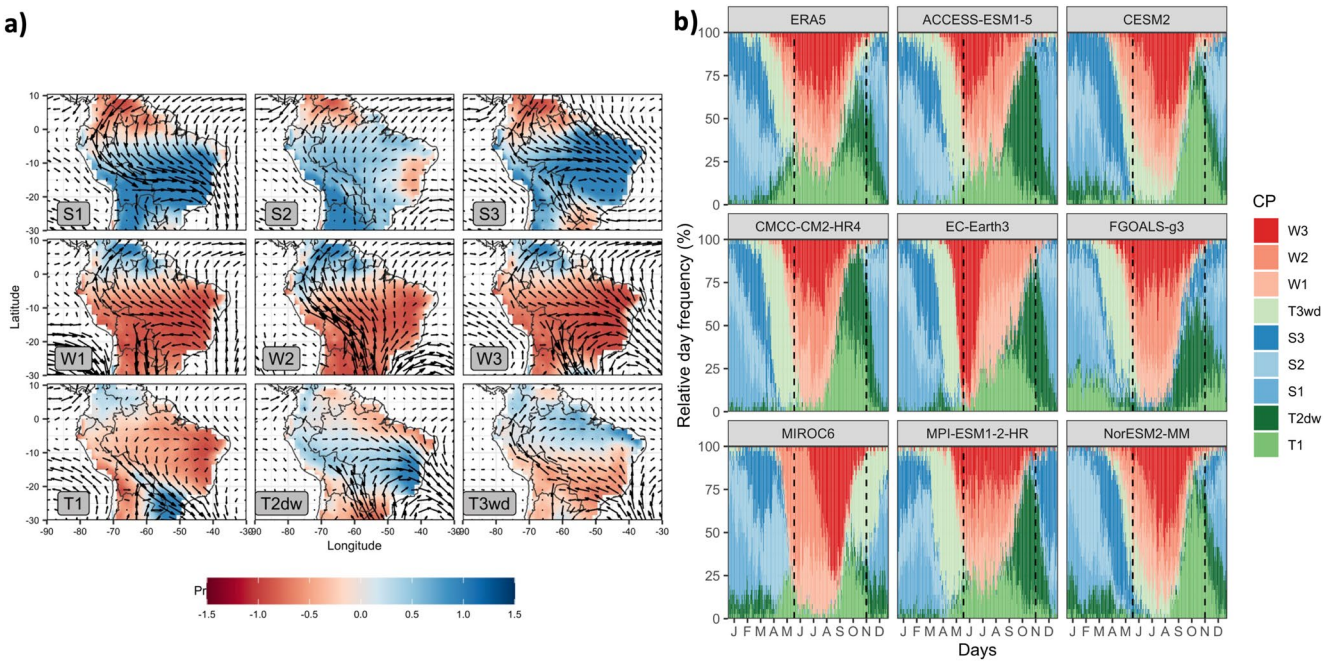

Figure 2. (a) Spatial patterns of low-level wind and rainfall anomalies (in m/s and mm/day vs. the annual mean) for the nine circulation-patterns (CPs) as depicted by the ERA5 reanalysis. Adapted from Espinoza et al. (2021), who identified three "winter" CPs (W1, W2 and W3), three "summer" CPs (S1, S2 and S3) and three "transitional" CPs (T1 and T2dw mostly for the dry-to-wet transition season and T3wd for the wet-to-dry transition season). Vectors indicate wind anomalies at 850 hPa and shaded colors refer to Climate Hazards Group Infrared Precipitation with Stations (CHIRPS) rainfall anomalies; (b) Seasonal cycle of the nine CPs as depicted by the ERA5 reanalysis and selected general circulation models (GCMs). The x-axis displays the 365 days of the year, while the y-axis indicates the relative mean daily frequency of each CP.

austral summer. For instance, this was the case of the CanESM5 and EC-Earth3 models, which presented relative minimum and maximum values by the end of the summer and autumn austral seasons, respectively (Figure 1a). Other models – such as MIROC6, MPI-ESM1-2-HR and NorESM2-MM – appropriately simulated the annual cycle, although they overestimated (underestimated) rainfall during late spring (winter). In fact, GCMs tended to underestimate PP throughout the year, more systematically during the austral winter. This general underestimation found in this set of CMIP6 is in agreement with previous studies analyzing GCM PP outputs over several parts of South America (Almazroui et al., 2021; Gulizia & Camilloni, 2015; Sierra et al., 2015), even though some improvements were made in CMIP6 simulations compared to the previous CMIP5 models (Meehl et al., 2020; Ortega et al., 2021). This may be due to deficiencies in the modeled deep convection and low-level tropospheric moisture (Sakaguchi et al., 2018).

In terms of the SAMS onset representation, GCMs tended to go from dry to wet conditions too quickly compared to the observations and, as described above, often started from drier conditions than observed during winter. Furthermore, models usually detected an earlier start of the wet season, of about three pentads of difference with CHIRPS (Figure 1b). On the other hand, SAMS demise presented more spread dates among models. Some of them – including CMCC-CM2-HR4 and EC-Earth3 – showed a late SAMS demise, thus resulting in an extended rainy season, whereas in other GCMs like MPI-ESM1-2-LR an early SAMS demise was found. These differences in the annual cycle evidence the GCMs limitations in simulating PP seasonality over southern Amazonia. In this regard, the use of model PP outputs for the selection of GCMs and for the understanding of physical processes of the SAMS is not advisable (Bettolli & Penalba, 2014; Fernández-Granja et al., 2021).

3.2. Identification of Circulation Patterns

As found by Espinoza et al. (2021) considering the 1979–2020 period, different seasonal CPs were identified over STSA (Figure 2a): three "winter" CPs (W1, W2 and W3), three "summer" CPs (S1, S2 and S3) and three "transitional" CPs (T1, T2dw for the dry-to-wet transition season and T3wd for the wet-to-dry transition season). A brief description of the ERA5 reanalysis-based CPs studied in that previous study is included below in Table 1

Table 1
Summary Table of the Main Features of the Circulation Patterns Over South Tropical South America (STSA) Identified by Espinoza et al. (2021), Who Described Three "Winter" Circulation-Patterns (CPs) (W1, W2 and W3), Three "Summer" CPs (S1, S2 and S3) and Three "Transitional" CPs (T1 and T2dw Mostly for the Dry-To-Wet Transition Season and T3wd for the Wet-To-Dry Transition Season)

		Intraseasonal variability		
	Summer CPs	S1	S2	S3
		-Anomalous northerly cross-equatorial winds.-Southerly wind intrusion over La Plata basin and cyclonic circulation over southern coastal Atlantic. -Convergence of low-level winds over the SACZ region.-SESA-SACZ precipitation dipole, related to the effect of extratropical Rossby wave-trains over the low-level circulation and differentiated convective activity.-Negative rainfall anomalies over northern South America	-Anomalous northerly cross-equatorial wind toward southeastern South America (SESA) related to SALLJ. -Anticyclonic circulation over the southern Atlantic Ocean.-Negative rainfall anomalies over northern South America.	-Anomalous northerly cross-equatorial winds. -Southerly wind intrusion over southern Amazon and cyclonic circulation over the SACZ region. -Convergence of the low-level flow over southern and eastern Amazonia.-SESA-SACZ precipitation dipole, related to the effect of extratropical Rossby wave-trains over the low-level circulation and differentiated convective activity.-Negative rainfall anomalies over northern South America.
Seasonal Variability	Winter CPs	W1	W2	W3
		-Anomalous southerly cross-equatorial wind. -Anticyclonic circulation over SESA related to SALLJ. -Low-level divergence over southwestern Amazon southern Amazonia-Negative (positive) rainfall anomalies over the entire STSA (northern South America).	-Southerly wind anomalies extended east of the Andes, often related to cold-surge intrusions. -Negative (positive) rainfall anomalies over the entire STSA (northern South America and northwestern Amazon).	-Anomalous southerly cross-equatorial wind.Anticyclonic circulation over the south tropical Atlantic, related to an intensified SALLJ. -Low-level divergence over southwestern Amazon. -Negative (positive) rainfall anomalies over the entire STSA (northern South America).
	Transitional CPs	T1	T2dw	T3wd
		-Intensified SALLJ from central Amazonia to southern La Plata basin, associated with an anomalous anticyclonic circulation over SACZ. -Southerly wind incursion over the east of the Andes and La Plata basin. -Convergence over the SESA region related to the SESA-SACZ dipole. -One of the main forcings of mesoscale convective systems responsible for heavy rainfall events in southeastern South America (SESA) during spring.	-Anomalous northerly cross-equatorial winds. -Southerly wind intrusion reaching southern Amazon, related to cyclonic circulation over the south tropical Atlantic Ocean. This feature is characteristic of frontal perturbations responsible for the positive rainfall anomalies over southern Amazon. -Wind convergence over southern Amazon and SACZ region.	-Anomalous southerly cross-equatorial winds. -Negative (positive) rainfall anomalies over the SACZ region and the southern Amazonia (northeastern Amazonia and northern South America). -Southerly wind intrusion in the Amazon basin.

for a better understanding of the process-based model evaluation performed here. A more detailed analysis of this classification and the underlying physical processes can be found in Espinoza et al. (2021).

It is interesting that the present classification of atmospheric circulation was able to identify the main atmospheric features that characterize the STSA climate and are associated with rainfall variability over the region, including the temporal variability of the SALLJ. Moreover, the main intraseasonal summer CPs include the SESA-SACZ PP dipole in S1, S2 and S3 and the variability of the SACZ itself (see Espinoza et al., 2021 and references therein).

In a following analysis, the spatio-temporal variability of the CPs as reproduced by the GCMs was assessed. The mean seasonal cycles of the relative frequency of CPs are illustrated for the ERA5 reanalysis and selected GCMs – depicting different performances – in Figure 2b (results for all GCMs analyzed in this study were included in Figure S1 as Supporting Information S1). As most of the temporal variation of CPs is mainly guided by planetary-scale features (e.g., solar radiation and the related meridional shift of the Intertropical Convergence Zone or ITCZ), we expect that GCMs capture the main features of seasonal variability over STSA. The ability to reproduce the seasonal behavior of the

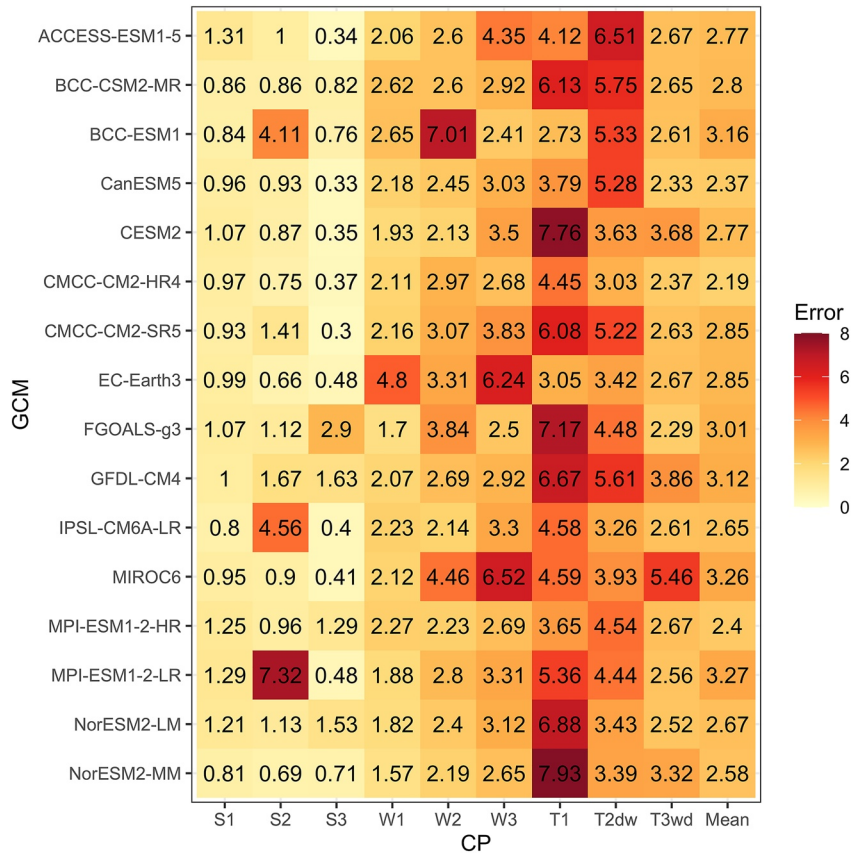

Figure 3. Absolute error values (expressed as number of days) in the representation of the seasonal cycle of the nine circulation-patterns (CPs) during the dry-to-wet transition season (July to October) in the different general circulation models (GCMs) compared to the ERA5 reanalysis. Last column corresponds to the mean value for each GCM.

CPs notably varied among GCMs. Models tended to have more difficulties in simulating the frequencies of transitional CPs, especially T1 and T2dw, which are particularly important for the initiation of the wet season. This is partly expected given that the seasonal cycle is considered in the definition of CPs. Hence, the transition between the winter and summer seasons (close to zero in the EOF space) is more challenging to reproduce. GCMs usually underestimated T1 during autumn, while they tended to overestimate T2dw during spring (see, for instance, ACCESS-ESM1-5 and CESM2). Other GCMs were not able to successfully reproduce the correct timing of these CPs, like GFDL-CM4, MPI-ESM1-2-LR (both shown in Figure S1 of Supporting Information S1) and FGOALS-g3, which indicated the occurrence of T1 with maximum frequency during summer.

GCMs performance was more precise in summer CPs compared to the transitional patterns as the GCMs were generally able to identify three CPs during this season (but often showing differences in their seasonal evolution), while most of them correctly identified three "winter" CPs, although differing in their maximum frequencies during this season compared to ERA5 (Figure 2). EC-Earth3 and MIROC6 misrepresented W3 as they strongly overestimated this pattern during the beginning and ending of the winter, respectively, and underestimated it during the rest of the season. In fact, the deficiencies of these GCMs were extended to the other CPs. EC-Earth showed a reduced seasonal variability of the CPs frequencies, with specific patterns dominating during extended periods as detected for T3wd. Note that this lack of temporal variability could also be found in other GCMs such as CMCC-CM2-SR5 (Figure S1 of Supporting Information S1).

In general terms, only a few GCMs - such as ACCESS-ESM1-5, CMCC-CM2-HR4, MPI-ESM1-2-HR (Figure 2b) and CanESM5 (Figure S1 of Supporting Information S1) were able to adequately simulate the CPs frequencies throughout the year, despite often presenting differences in the timing and/or maximum frequencies of specific CPs. Additionally, in order to measure the models' performance in simulating the seasonal cycle of CPs, Figure 3 displays the error metric as described in Section 2.4. This metric was estimated for each CP, individually, and a

mean value was calculated from them. Focus was put on the representation of the dry-to-wet transition season. GCMs presented higher errors during the transition patterns T1 and T2dw – such as NorESM2-MM and CESM2 for T1 – while the smallest errors were found for the summer CPs. Note that this is somehow expected given that those patterns were the least frequent during this season, thus contributing less to the error measure. However, a few GCMs like BCC-ESM1 and MPI-ESM1-2-LR presented large errors for S2 – with error values from 4 to 7 days – indicating a poor representation of the CPs seasonal cycle. When evaluating the mean error (last column in Figure 3), the best ranked GCMs were CMCC-CM2-HR4, CanESM5, MPI-ESM1-2-HR – with error values of about 2 and 3 days – in agreement with the visual inspection of the seasonal cycles of Figure 2b. This evaluation, however, is not robust enough to state that these GCMs are the best ones but offers a general overview of CPs frequency and is a valuable tool to consider in the next analyses.

The GCMs representation of the nine CPs spatial patterns of 850 hPa wind anomalies was summarized through Taylor diagrams (Figure 4). Each GCM is represented by one numbered and colored point in the plot. The closer the GCM point is located to the ERA5 reference (black point), the better is the model performance. As evidenced in the previous analysis, models exhibited a more accurate performance in winter and summer CPs than in transitional CPs. During those seasons - but especially in winter - model agreement was larger as seen by the small spread in the clouds of points. Models usually presented spatial correlation values of about 0.7 and standard deviations around 1, although some GCMs tended to underestimate (overestimate) the spatial variability of the CPs - standard deviation below (above) 1 - during winter (summer) CPs. For instance, the models with better performance during winter included CanESM5, CMCC-CM2-HR4, CESM2 and NorESM2-MM, whereas BCC-ESM1, EcEarth-3 and IPSL-CM6A-LR and MPI-ESM1-2-HR showed lower skills, with reduced correlation values and standard deviations of about 0.6 (Figure 4). For summer CPs, despite more varied performances between models and the different summer patterns (especially in S2), good performances could be found for the ACCESS-ESM1-5 and CMCC-CM2-HR4 models, while BCC-ESM1, BCC-CSM2-MR and MPI-ESM1-2-LR exhibited some of the poorest scores. In the case of transitional patterns, models CMCC-CM2-HR4 and CanESM5 adequately reproduced the low-level wind spatial structures, followed by CESM2 and NorESM2-MM. Recall that these models were formerly identified within the best performances in the representation of the CPs seasonality (Figures 2a and 3), which, altogether, is a good indicator of their capabilities in reproducing the main atmospheric states over STSA, especially during the transition seasons. On the other hand, MPI-ESM1-2-LR, MIROC6, FGOALS-g3 and BCC-CSM2-MR typically showed the poorest spatial representations of these CPs, in line with their limited performance in the temporal variability of CPs.

For a deeper insight on the models' spatial reproduction of CPs, the spatial patterns of 850 hPa wind and rainfall anomalies of W3, T2dw and S1 – representing the winter conditions that precede the SAMS onset, the SAMS early initiation and its mature phase, respectively – are illustrated in Figure 5 for a few models exhibiting different performances as described in the previous analyses. The complete set of GCMs and CPs can be found in Figure S2 of the Supporting Information S1. As shown in the Taylor diagrams from Figure 4, the low-level circulation in W3 was well-reproduced by the GCMs, particularly the southerly wind anomalies from the Bolivian Amazon to southeastern South America (SESA), even though some of them - such as EC-Earth3 and MPI-ESM1-2-HR - depicted the anomalous anticyclonic center over the south Atlantic Ocean strengthened and located further to the northwest compared to ERA5. Furthermore, these GCMs simulated larger wind anomalies to the north than ERA5. The PP pattern related to T2dw was adequately represented, indicating negative anomalies over most of STSA apart from northern South America and SESA. When analyzing T2dw and S1, models presented more difficulties in simulating T2dw – associated with the SAMS onset – than S1, in which the monsoon is close to its mature phase. On one hand, the extratropical anomalous southerly winds of T2dw were correctly reproduced by CESM2, followed by CMCC-CM2-HR4, which exhibited weaker anomalies than ERA5. This is a key mechanism for the SAMS onset as these southerly winds provide suitable large-scale thermodynamic conditions to trigger PP (Li & Fu, 2006; Wang & Fu, 2004). On the other hand, the low-level flow to the east of Brazil – associated with positive rainfall anomalies in this region – was well-represented by the different GCMs, although they often differed in the magnitude of these anomalies, like CESM2, CMCC-CM2-HR4 and EC-Earth3 (Figure 5). Other models such as NorESM2-LM and NorESM2-MM were able to simulate the low-level circulation observed in T2dw, although NorESM2-LM exposed more differences, particularly over central Amazonia (Figure S2 in Supporting Information S1). The SESA-SACZ dipole was well reproduced by models such as CESM2, CMCC-CM2-HR4 and NorESM2-MM, in line with their ability to reproduce the associated atmospheric circulation. S1 anomalous northerly low-level winds were well-captured by most of the GCMs, whereas the simulation of the

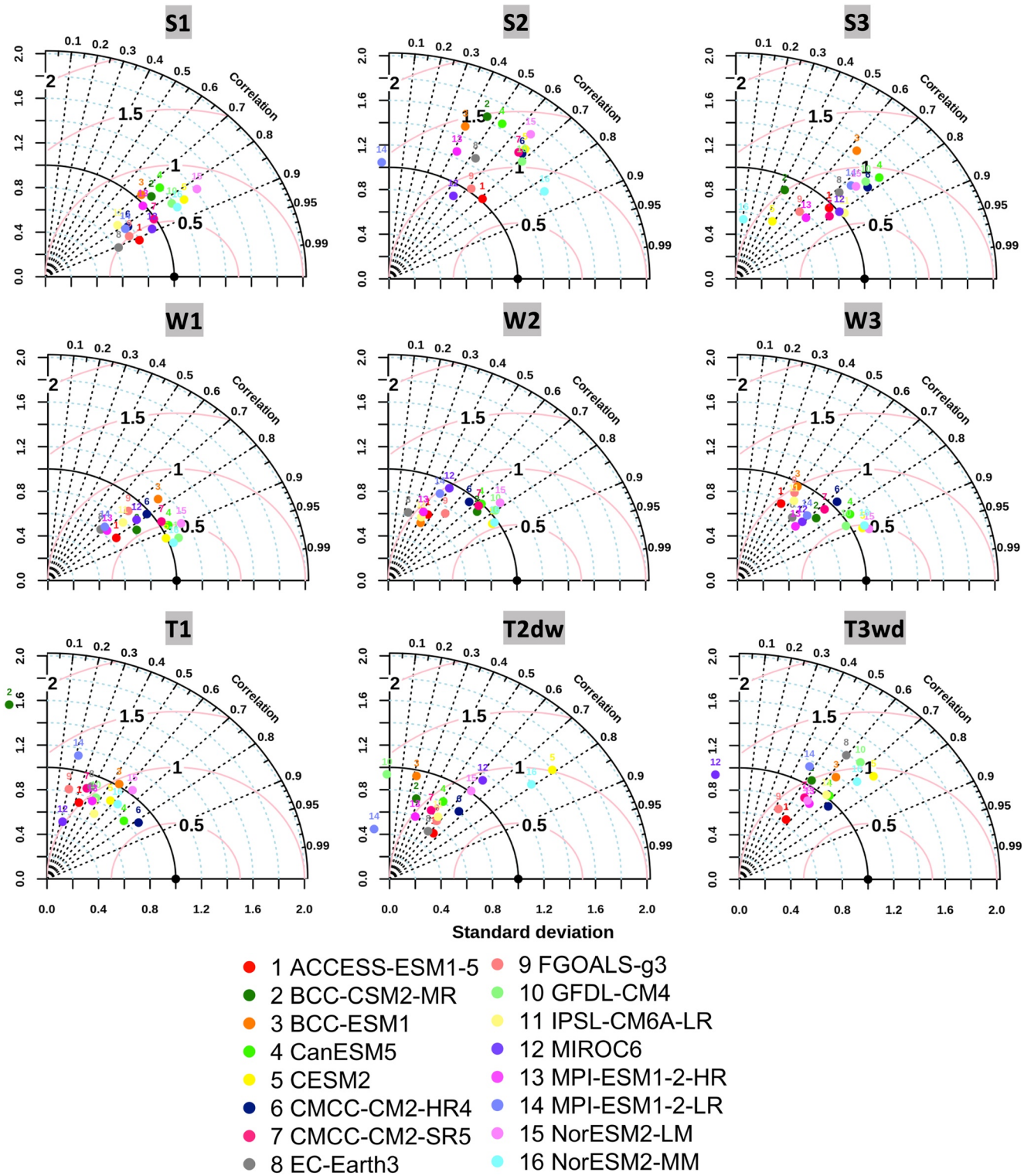

Figure 4. Taylor diagrams of the spatial patterns of low-level wind anomalies at 850 hPa for the nine circulation-patterns (CPs). GCMs are indicated in numbered and colored poins and the black point refers to the ERA5 reference.

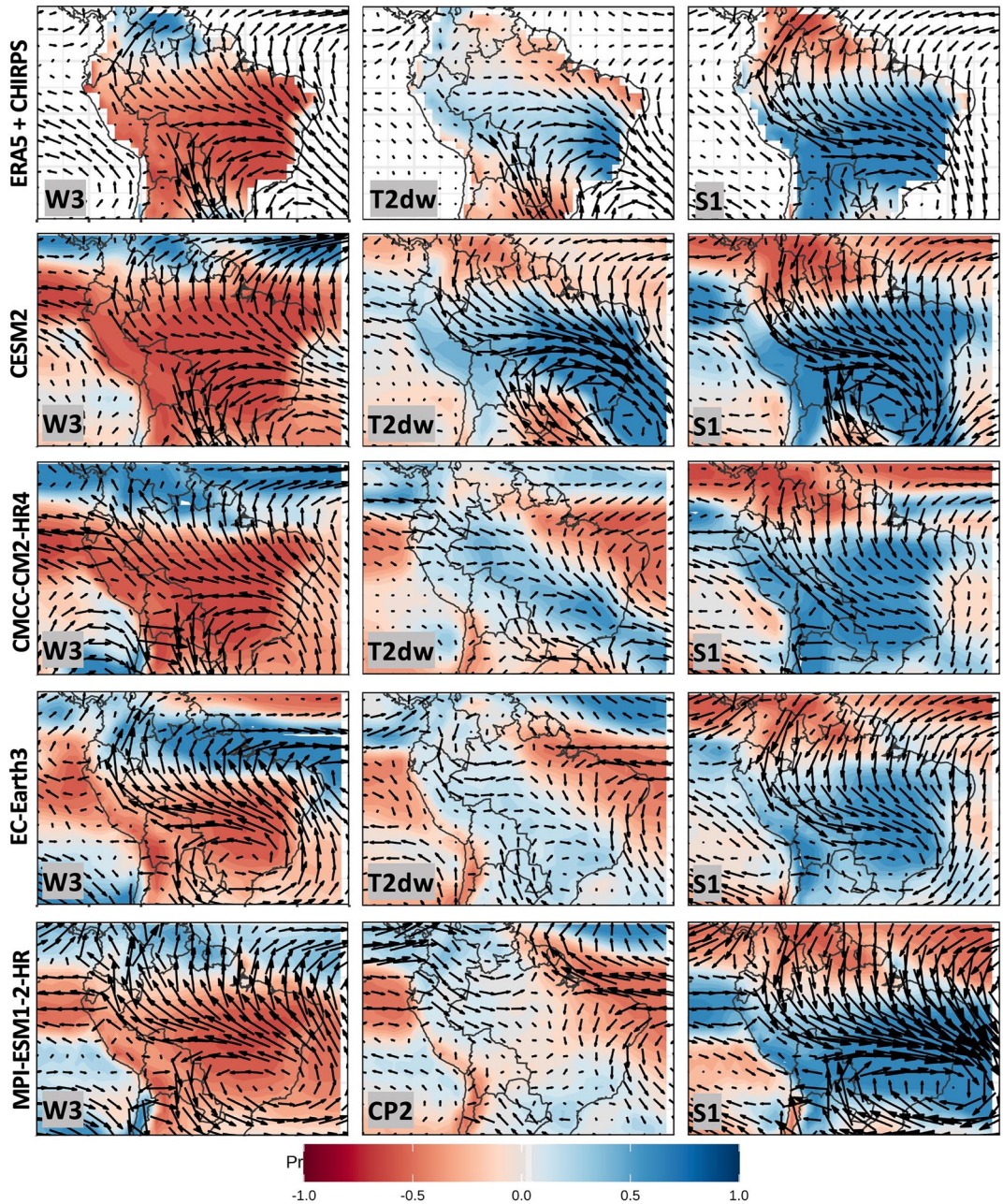

Figure 5. Spatial patterns of 850 hPa wind and rainfall anomalies for W3, T2dw and S1 - representing the winter conditions that precede the South American Monsoon System (SAMS) onset, the SAMS early initiation and its mature phase, respectively - as depicted by the ERA5 and Climate Hazards Group Infrared Precipitation with Stations (CHIRPS) reference datasets and a few selected general circulation models (GCMs). Vectors indicate wind anomalies at 850 hPa and shaded colors refer to rainfall anomalies versus each GCM and ERA5 long-term means.

southerly wind anomalies varied more among models, with some of them not being able to capture low-level wind direction, like BCC-ESM1 and FGOALS-g3 (Figure S2 in Supporting Information S1). GCMs – such as CESM2 and MPI-ESM1-2-HR – tended to intensify S1 wind anomalies and anomalous cyclonic circulation in southeastern STSA compared to ERA5.

The results discussed above highlight the relevance of low-level circulation in understanding whether the GCMs are able to simulate the SAMS onset as well as the spatio-temporal variability of PP. Moreover, the weather types identified using low-level circulation span the main atmospheric configurations over STSA and can potentially

organize structures at larger scales, helping to comprehensively understand the atmospheric processes on the mid and high-level atmosphere. For this reason, wind composites at 250 hPa of each CP were constructed and presented for ERA5 and selected GCMs in Figure S3 (see Supporting Information S1). As found by Espinoza et al. (2021), winter CPs were characterized by subtropical upper-level westerlies south of 10°S, which were successfully captured by the set of GCMs, while for summer CPs the presence of the Bolivian high – particularly in S3 – dominated together with easterly winds over the tropical Andes. These features were captured by the GCMs, although some of them simulated the Bolivian high with less intensity than the ERA5 reanalysis, like ACCESS-ESM1-M and CESM2. During transitional CPs, the subtropical westerlies were identified in both ERA5 and GCMs with greater intensity in the dry-to-wet transition patterns T1 and T2dw. GCMs can realistically simulate the large-scale features of atmospheric circulation, evidencing stronger deficiencies in the lower levels due to the models not being able to capture features such as topographic gradients and land-ocean contrasts (Ambrizzi et al., 2018). In this way, GCMs performance in the upper atmosphere seemed better compared to the low-level circulation, as analyzed here.

To finalize this assessment, pressure-latitude cross-section patterns of zonal wind anomalies (shaded colors) and meridional-vertical wind anomalies averaged over 70°–40°W were explored in W3, T2dw and S1 (Figure 6 and Figure S4 of the Supporting Information S1). According to the ERA5 reference data set, W3 was identified with upward motion and easterly wind anomalies in the lower and middle atmosphere in 0–10°N, associated with positive rainfall anomalies found in that region (Figure 2a). In the extratropics (20°–40°S), subsidence predominated from 500 hPa to the surface level related to negative PP anomalies there. As observed in Figure S3 of Supporting Information S1, the subtropical jet was also detected in the upper atmosphere, according to the positive zonal wind anomalies over this band of latitudes. The set of GCMs adequately reproduced these vertical structures in terms of the wind magnitude and direction, with some differences near the surface, like MPI-ESM1-2-HR in the extratropics and CESM2 over 0–10°N. T2dw and S1 exhibited ascending motion at the different pressure levels evaluated over southern Amazonia (bounded by red dashed lines in Figure 6) and the continental SACZ region, where rainfall anomalies were positive. This pattern was more intense for S1 than for T2dw, in accordance with a more developed SAMS. On the contrary, downward motion was detected in the extratropics (20°–40°S) and the Northern Hemisphere of South America - particularly during T2dw – where rainfall anomalies were negative, leading to the SESA-SACZ dipole structure previously mentioned. Note that, although the Bolivian high can be detected more clearly in summer patterns like S3 (Figure S3 in Supporting Information S1), the associated anticyclonic circulation can also be observed – with less intensity – in T2dw and S1 and identified in the vertical patterns of Figure 6, approximately where the zonal wind anomalies at the upper atmosphere change of sign. This could be found near 15°S in T2dw and located more to the south in S1, as depicted by the ERA5 reanalysis. In the case of the selected GCMs, a good correspondence with the reference patterns was found, presenting more discrepancies in the lowest atmospheric levels, especially in the extratropics for T2dw. This could be associated with the models' limitations in simulating the low-level circulation and associated PP pattern typical of the SAMS onset, as analyzed in Figures 4 and 5. In addition, most of the models tended to intensify the negative wind anomalies in the middle and upper atmosphere over southern Amazonia in S1, although the overall structure was satisfactorily captured.

3.3. Circulation Patterns and Associated Rainfall During the Dry-To Wet Transition Season

In order to further evaluate the link between large-scale atmospheric features and interannual rainfall variability over STSA during the dry-to-wet transition season, a detrended correlation analysis was carried out between the interannual time series of the frequency of W3 and T2dw and two rainfall indices – mean seasonal PP and dry-day frequency (PP and DDF, respectively) – as described in Section 2.4. Note that focus was put specifically on these two CPs since they were associated with the lengthening of the dry season over STSA as shown by Espinoza et al. (2021).

According to the reference datasets (ERA5 and CHIRPS), the years with an anomalous higher-than-usual frequency of W3 were characterized by negative PP and positive DDF anomalies over southeastern Amazonia and the SACZ region, as depicted by negative and positive correlation values, respectively, in Figure 7 (first row). Conversely, the signals were reversed and less significant when analyzing T2dw, with positive (negative) correlations over eastern Brazil and negative (positive) correlations over northern South America for PP (DDF). Note that these associations between the variability of the frequency of the CPs and rainfall relate to the physical

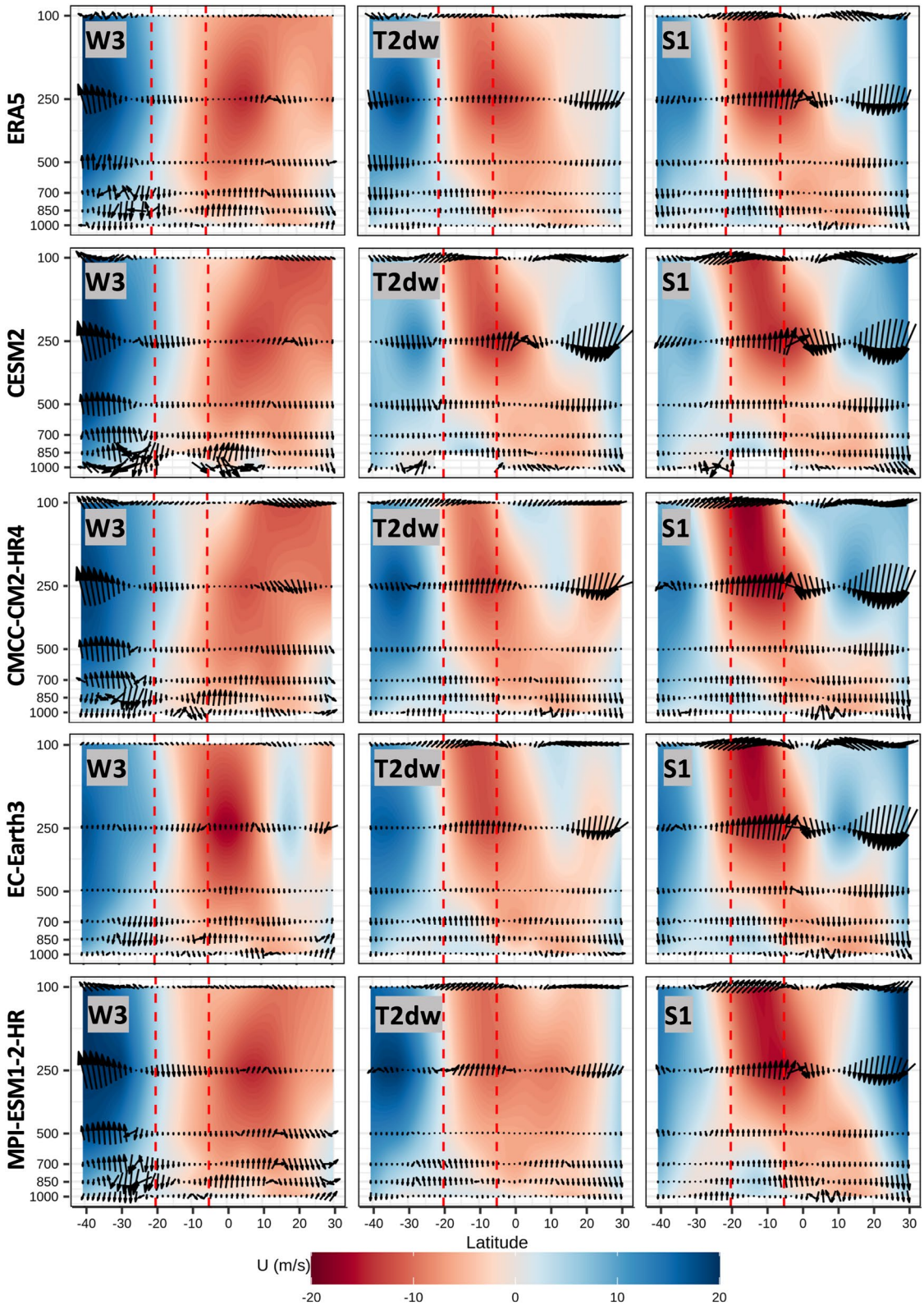

Figure 6. Pressure–latitude cross-section of zonal wind anomalies (shaded colors) and meridional-vertical wind anomalies (vectors) zonally averaged over the 70°W–40°W region. Results are shown for W3, T2dw and S1 as depicted by the ERA5 and Climate Hazards Group Infrared Precipitation with Stations (CHIRPS) reference datasets and a few selected general circulation models (GCMs). Vertical red dashed lines indicate the boundaries of the southern Amazon (5°S–20°S).

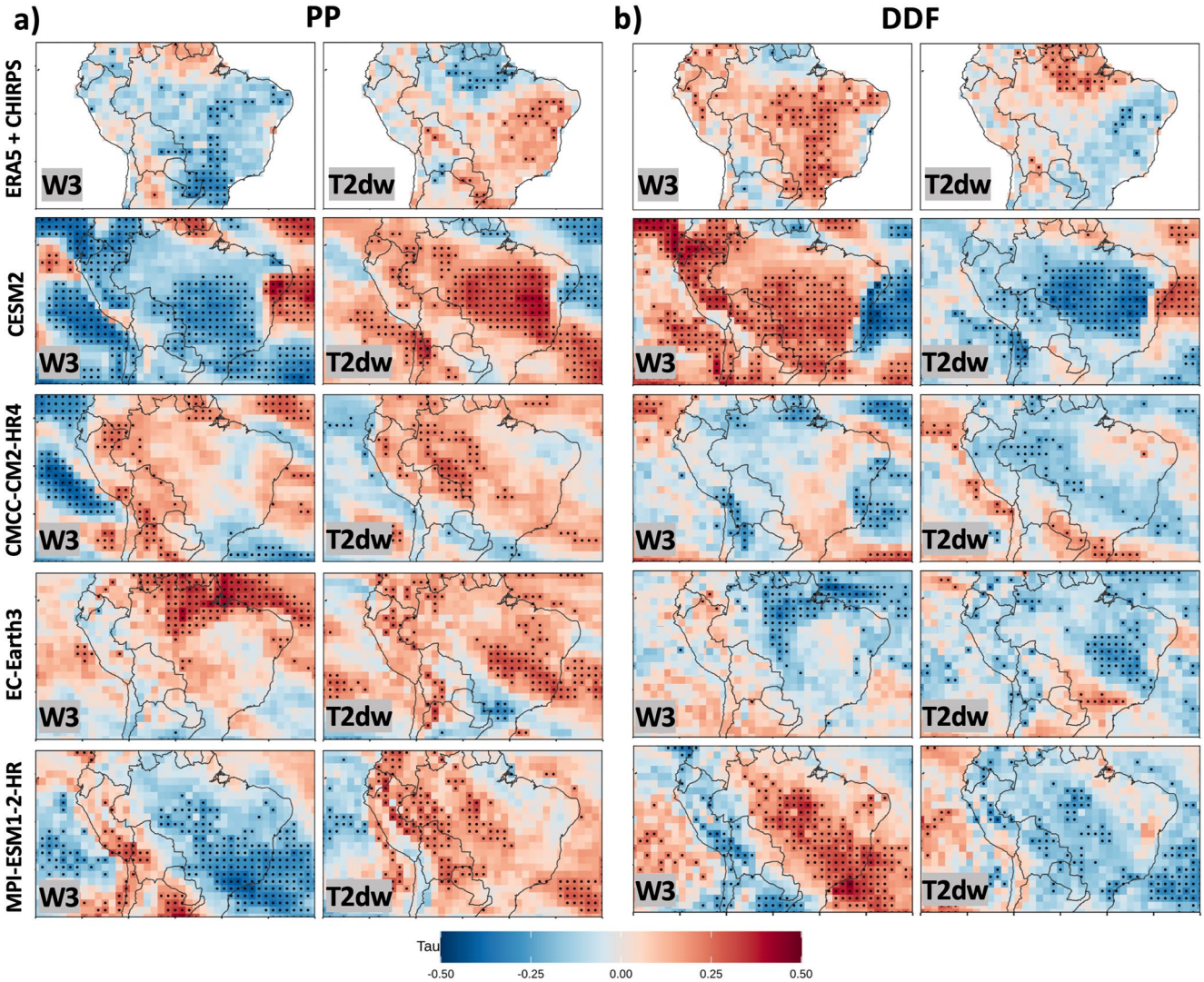

Figure 7. Kendall-Tau correlation values between the interannual time series during the dry-to-wet transition season (July to October 1979–2014) of the frequency of W3 and T2dw and: (a) the mean seasonal rainfall Precipitation (PP); (b) the dry-day frequency (DDF). Results are shown for the ERA5 + CHIRPS reference and a few selected general circulation models (GCMs). Grid cells with significant correlation values are marked with dots.

processes behind W3 and T2dw - the enhancement of the SALLJ and the southerly cold-air intrusions, respectively - that lead to PP occurrence over STSA (Figures 2b and 6). This analysis was performed for all CPs but the main signals during the dry-to-wet transition season were detected in W3 and T2dw (not shown).

The spatial pattern of correlation values related to PP and DDF were generally well-simulated by the GCMs, particularly by CESM2 that, despite overestimating the spatial extent and significance of these relationships, successfully captured the relationship between low-level winds and PP in W3 and T2dw (Figure 7). CMCC-CM2-HR4 and MPI-ESM1-2-HR agreed with the differentiated signals of these patterns but presented more differences in the location and/or significance of the maximum correlation values. The EC-Earth3 model managed to represent the rainfall association with T2dw over eastern Brazil but was not able to reproduce the links detected for W3, as this model exhibited positive (negative) correlations for PP (DDF) over most of Brazil, with statistical significance in the northern part of the domain, contrary to the reference datasets. This was probably related to the EC-Earth3 poor representation of the temporality of the CPs, especially the timing and predominance of W3 during winter (Figure 2b).

Finally, considering model capabilities in the different aspects studied in Section 3.1 and the correlation analysis described above – including the representation of the timing and the main spatial features of CPs – we selected

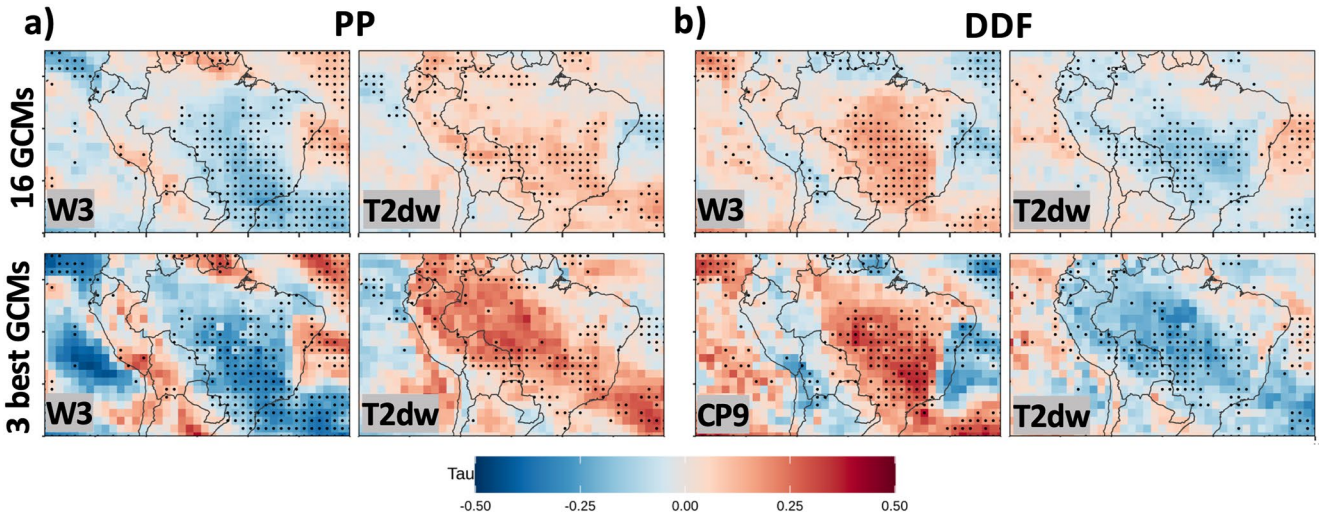

Figure 8. Kendall-Tau average correlation values between the interannual time series during the dry-to-wet transition season (July to October 1979–2014) of the frequency of W3 and T2dw and: (a) the mean seasonal rainfall Precipitation (PP); (b) the dry-day frequency (DDF). Averages were estimated for the set of 16 general circulation models (GCMs) and for the 3-best GCMs (CESM2, CMCC-CM2-HR4 and MPI-ESM1-2-HR), separately. Grid cells with model agreement in the sign of the correlation values above 75% (considering the complete 16 GCMs set) are marked with dots.

three GCMs that performed best throughout this assessment: CESM2, CMCC-CM2-HR4 and MPI-ESM1-2-HR. Thereby, based on the complete set of 16 GCMs employed here and the 3-best GCMs, a similar analysis was performed considering the average correlation values of these model ensembles (Figure 8). Moreover, model agreement in the sign of these correlations above 75% was highlighted with dots. This analysis evidenced that, considering the complete set of 16 GCMs, the main relationships between W3 and T2dw frequencies and both PP indices was well-captured in terms of the sign of the correlations and the location of the maximum values. The negative (positive) signals over southern and central Brazil for PP (DDF) were correctly described by the GCMs, presenting more difficulties in reproducing the spatial variability in these indices when linked to T2dw. However, these average correlations were lower than the ones found in ERA5 or in individual GCMs – with maximum values around 0.3 in the model ensemble compared to correlations up to 0.6 in ERA5 – due to the use of a multi-model ensemble of 16 GCMs, which includes some models with poor or regular performances throughout their evaluation. This was upgraded when considering only the 3-best GCMs: the average correlations were increased – approximately from 0.3 to 0.5 – showing a strengthened relationship between CP frequencies and rainfall over STSA (recall that the individual correlation patterns for each of the 3-best GCMs are displayed in Figure 7). These analyses highlight that the variability of the frequency of W3 and T2dw modulates rainfall variability during the dry-to-wet transition period over southeastern Amazonia and the SACZ region, and that the different GCMs were generally able to reproduce this large-scale circulation related to the PP regime of STSA.

4. Summary and Final Remarks

Emerging recognition has been seen on the effects of climate change in STSA as ongoing changes in its hydro-climatic regimes and weather patterns have been identified, including a lengthening of the dry season associated with a delayed onset of the SAMS (e.g., Arias et al., 2015; Caballero et al., 2022; Correa et al., 2021; Debortoli et al., 2015; Espinoza et al., 2021; Fu et al., 2013; Jones & Carvalho, 2002; Marengo et al., 2012; Pascale et al., 2019; Wongchuig et al., 2021). Moreover, deforestation and climate change are altering the Amazon rainforest, promoting an ecosystem stress favoring biomass loss, tree mortality and fire activity (Gatti et al., 2021; Reis et al., 2018; Silva et al., 2020). Thereby, studying the role of large-scale climate variability on the SAMS onset can provide additional information to understand the related impacts documented over the recent years and projected for the 21st century.

The foregoing context motivates this study, which aimed to evaluate the performance of a set of 16 CMIP6 GCMs in terms of how well they reproduced the main atmospheric states and their related rainfall patterns during 1979–2014 over STSA, based on the weather-typing approach proposed by Espinoza et al. (2021). Focus was put

on the representation of the CPs during the dry-to-wet transition season (July–October). Nine CPs were defined based on a k-means clustering of low-level wind anomalies, considering the daily ERA5 atmospheric circulation and CHIRPS rainfall data as reference.

In the first place, an analysis of the PP annual cycle over southern Amazonia showed that GCMs tended to underestimate PP throughout the year – and more systematically during the austral winter – and evidenced their limitations in simulating rainfall variability, in agreement with previous studies (Almazroui et al., 2021; Ortega et al., 2021; Sierra et al., 2015). GCMs tended to go from dry to wet conditions too quickly, evidencing deficiencies in the representation of the SAMS onset. Note, however, that a simplified interpretation of the SAMS onset and demise was considered here for the purpose of model evaluation, whereas more comprehensive definitions are presented in the literature (Arias et al., 2015; Bombardi et al., 2020). On the other hand, the rationale behind the misrepresentation of rainfall features could be some limitations in model parameterizations and representation of atmospheric moisture transport and deep convection (Sakaguchi et al., 2018). In this regard, the use of PP model outputs without taking into consideration their representation of the associated physical mechanisms may introduce important errors as the GCMs have clear limitations in reproducing even the PP annual cycle.

When evaluating the spatio-temporal variability of CPs, only a few GCMs correctly represented the different CPs and their seasonal variability. Model performance depended on the seasonal cycle and spatial structure of the CPs. Some of the GCMs adequately reproduced the frequencies of CPs, with lower skills in the transition seasons. GCMs typically depicted reduced seasonal variability, like the case of EC-Earth3. Only a few GCMs were able to adequately simulate the CPs frequencies throughout the year – such as ACCESS-ESM1-5, MPI-ESM1-2-HR and CMCC-CM2-HR4 – despite presenting differences in specific CPs, such as in the timing and/or the maximum frequency values of winter CPs – especially W3 – in the two first models and in the low frequency of the transitional CPs (T1 and T2dw) during autumn in the last one. In terms of the spatial patterns, models tended to better reproduce winter structures, while the transitional CPs exhibited more differences due to a poor representation of the southerly wind intrusions to STSA and the seasonal variability of the South American low-level jet, which are characteristic of the dry-to-wet transition period. The CESM2 and CMCC-CM2-HR4 models exhibited the best performances, adequately reproducing not only the low-level winds and rainfall patterns but also the atmospheric circulations at different levels. Other models like CanESM5 and NorESM2-MM also well-reproduced these features, in agreement with their performances on the temporal variability of the CPs. On the contrary, some GCMs like MPI-ESM1-2-LR and MIROC6 exhibited the poorest spatial representations of these transitional CPs, in line with their limited performance on the seasonal behavior of the CPs. Moreover, the variability of the frequency of specific patterns during this transitional period (W3 and T2dw) modulated rainfall variability over southeastern Amazonia and the SACZ region. This was generally captured by the different GCMs, being the representation by CESM2 and MPI-ESM1-2-HR the most accurate ones.

The results discussed above highlight the relevance of low-level circulation in understanding whether the GCMs are able to simulate the SAMS onset as well as the spatio-temporal variability of PP. This study allowed us to identify the best GCMs in terms of their representation of the atmospheric CPs associated with the development of the wet season in STSA, which has profound impacts on the changes in the hydrological cycle detected over the Amazonia. Furthermore, the interannual variability of the wet season over monsoonal regions is dependent of different climatic features such as local thermodynamic conditions, ocean-land atmospheric fluxes and the El Niño teleconnection, which remarks the complexity of assessing the SAMS features and their representation by GCMs (Bombardi et al., 2020; Londoño-Arteaga & Lima, 2021).

Additionally, it is interesting to mention the role of models' native resolution on their performance as evaluated here. In general terms, models with the finest native resolutions did not always depict the best performances, like the case of EC-Earth3. However, some of the GCMs recognized as the least skillful in simulating the CPs over STSA - such as FGOALS-g3 and GFDL-CM4 - presented the lowest spatial resolutions. When comparing GCMs from the same modeling institutes, the higher-resolution GCM usually exhibited a better performance than the lower-resolution GCM, like the MPI-ESM1-2-HR and MPI-ESM1-2-LR models and the NorESM2-LM and NorESM2-MM models. This improved performance may be probably due to more complex parametrizations and representations of the different interactions involved in the climatic system (Eyring et al., 2016), although exploring the rationale behind the different GCMs representation of these mechanisms is beyond the scope of this study. The GCMs that were found to adequately simulate the main atmospheric circulation features in STSA were CESM2, CMCC-CM2-HR4 and MPI-ESM1-2-HR, which are recommended to consider in follow-up studies on

the spatio-temporal variability of rainfall, its associated atmospheric environment, and its related impacts under a climate change scenario.

Note that there are several documented procedures and ranking metrics used by different authors – which can be useful to assess model skills – based on the reproduction of surface variables and/or physical mechanisms (Coelho et al., 2021; Londoño-Arteaga & Lima, 2021; Wang et al., 2018). In this sense, the evaluation framework employed in this work focuses on the capability of the GCMs to represent the main atmospheric features in STSA through a weather-typing approach. This sort of process-based model evaluation offers a valuable source of information for designing high-resolution modeling experiments which, by relying on course-resolution information – typically from GCMs – for nesting the regional models with large-scale boundary conditions, may be affected by the GCM atmospheric circulation biases (Fernández-Granja et al., 2021; Maraun et al., 2021). In this sense, GCMs representation of sea surface temperature (SST) should be also considered in future studies as specific SST patterns over the Atlantic Ocean preceding the wet-season onset can influence the SAMS development (Yin et al., 2014). Likewise, given the projections of drying conditions over STSA (Almazroui et al., 2021; Parsons, 2020; Sena & Magnusdottir, 2020; Thaler et al., 2021; Wainwright et al., 2021), these findings motivate the study of the CPs changes during the 21st century in terms of their frequency, intensity, and associated rainfall, which will be addressed in future research.

Data Availability Statement

The different datasets used in this study are available online. ERA5 reanalysis [Data set] (Hersbach et al., 2020): https://www.ecmwf.int/en/forecasts/datasets/reanalysis-datasets/era5. CHIRPS V2.0 [Data set] (Funk et al., 2014): https://data.chc.ucsb.edu/products/CHIRPS-2.0/global_daily/.

Acknowledgments
This research has been supported by the French AMANECER-MOPGA project funded by ANR and IRD (ANR-18-MPGA-0008), and by the ACE-Amazon project funded by the regional program CLIMAT-AmSud (21-CLIMAT-01). M.E. Olmo, M.L. Bettolli and R. Balmaceda-Huarte have been funded by the Argentinian projects 2018-20020170100117BA, 20020170100357BA from the University of Buenos Aires and the ANPCyT PICT-2018-02496 and PICT 2019-02933. J-C. Espinoza received support from project No. 077-2021 PROCIENCIA (FONDECYT)-/BM. P.A. Arias has been funded by MINCIENCIAS through the grants No. 80740-490-2020 and No. 80740-238-2021. The authors acknowledge the WCRP CMIP6 for producing and making available the model outputs used in this work.

References

Almazroui, M., Ashfaq, M., Islam, M. N., Rashid, I. U., Kamil, S., Abid, M. A., et al. (2021). Assessment of CMIP6 performance and projected temperature and precipitation changes over South America. *Earth Systems and Environment*, *5*, 155–183. https://doi.org/10.1007/s41748-021-00233-6

Alves, L., Marengo, J., Fu, R., & Bombardi, R. (2017). Sensitivity of Amazon regional climate to deforestation. *American Journal of Climate Change*, *6*(01), 75–98. https://doi.org/10.4236/ajcc.2017.61005

Ambrizzi, T., Reboita, M. S., Porfirio da Rocha, R., & Llopart, M. (2018). The state-of-the-art and fundamental aspects of regional climate modeling in South America. *Annals of the New York Academy of Sciences*, *1436*(1), 98–120. https://doi.org/10.1111/nyas.13932

Arias, P. A., Fu, R., Vera, C. S., & Rojas, M. (2015). A correlated shortening of the North and South American monsoon seasons in the past few decades. *Climate Dynamics*, *45*(11–12), 3183–3203. https://doi.org/10.1007/s00382-015-2533-1

Arias, P. A., Garreaud, R., Poveda, G., Espinoza, J. C., Molina-Carpio, J., Masiokas, M., et al. (2021). Hydro-climate of the andes part II: Hydro-climate variability and sub-continental patterns. *Frontiers of Earth Science*, *8*, 505467. https://doi.org/10.3389/feart.2020.505467

Arias, P. A., Martínez, J. A., Mejía, J. D., Pazos, M. J., Espinoza, J. C., & Wongchuig-Correa, S. (2020). Changes in normalized difference vegetation index in the Orinoco and Amazon River basins: Links to tropical Atlantic surface temperatures. *Journal of Climate*, *33*(19), 8537–8559. https://doi.org/10.1175/jcli-d-19-0696.1

Arias, P. A., Ortega, G., Villegas, L. D., & Martínez, J. A. (2021). *Colombian climatology in CMIP5/CMIP6 models: Persistent biases and improvements* (Vol. 100, pp. 75–96). Revista Facultad de Ingeniería, Universidad de Antioquia.

Bettolli, M. L., & Penalba, O. C. (2014). Synoptic sea level pressure patterns - Daily rainfall relationship over the Argentine Pampas in a multi-model simulation. *Meteorological Applications*, *21*(2), 376–383. https://doi.org/10.1002/met.1349

Boisier, J. P., Ciais, P., Ducharne, A., & Guimberteau, M. (2015). Projected strengthening of Amazonian dry season by constrained climate model simulations. *Nature Climate Change*, *5*(7), 656–660. https://doi.org/10.1038/nclimate2658

Bombardi, R. J., Kinter, J. L., III, & Frauenfeld, O. W. (2019). A global gridded dataset of the characteristics of the rainy and dry seasons. *Bulletin of the American Meteorological Society*, *100*(7), 1315–1328. https://doi.org/10.1175/bams-d-18-0177.1

Bombardi, R. J., Moron, V., & Goodnight, J. S. (2020). Detection, variability, and predictability of monsoon onset and withdrawal dates: A review. *International Journal of Climatology*, *40*(2), 641–667. https://doi.org/10.1002/joc.6264

Caballero, C. B., Ruhoff, A., & Biggs, T. (2022). Land use and land cover changes and their impacts on surface-atmosphere interactions in Brazil: A systematic review. *The Science of the Total Environment*, *808*, 152134. https://doi.org/10.1016/j.scitotenv.2021.152134

Cahynová, M., & Huth, R. (2016). Atmospheric circulation influence on climatic trends in Europe: An analysis of circulation type classifications from the COST733 catalogue. *International Journal of Climatology*, *36*(7), 2743–2760. https://doi.org/10.1002/joc.4003

Carvalho, L., Jones, C., & Liebmann, B. (2004). The South Atlantic convergence zone: Intensity, form, persistence, and relationships with intraseasonal to interannual activity and extreme rainfall. *Journal of Climate*, *17*(1), 88–108. https://doi.org/10.1175/1520-0442(2004)017<0088:tsaczi>2.0.co;2

Carvalho, L. M. V., & Silva-Dias, M. A. F. (2021). Mesoscale and high-impact weather in the South American monsoon. *The Multiscale Global Monsoon System*.

Cavalcante, R. B. L., da Silva Ferreira, D. B., Pontes, P. R. M., Tedeschi, R. G., da Costa, C. P. W., & de Souza, E. B. (2020). Evaluation of extreme rainfall indices from CHIRPS precipitation estimates over the Brazilian Amazonia. *Atmospheric Research*, *238*, 104879. https://doi.org/10.1016/j.atmosres.2020.104879

Coelho, C. A. S., de Souza, D. C., Kubota, P. Y., Cavalcanti, I. F. A., Baker, J. C. A., Figueroa, S. N., et al. (2021). Assessing the representation of South American monsoon features in Brazil and U.K. climate model simulations. *Climate Resilience and Sustainability*, *1*, 1–23. https://doi.org/10.1002/cli2.27

Correa, I. C., Arias, P. A., & Rojas, M. (2021). Evaluation of multiple indices of the South American monsoon. *International Journal of Climatology*, *41*(S1), 2801–2819. https://doi.org/10.1002/joc.6880

Costa, M. H., & Pires, G. (2010). Effects of Amazon and Central Brazil deforestation scenarios on the duration of the dry season in the arc of deforestation. *International Journal of Climatology*, *30*(13), 1970–1979. https://doi.org/10.1002/joc.2048

D'onofrio, A., Boulanger, J. P., & Segura, E. C. (2010). CHAC: A weather pattern classification system for regional climate downscaling of daily precipitation. *Climate Change*, *98*(3–4), 405–427. https://doi.org/10.1007/s10584-009-9738-4

da Anunciação, Y. M. T., Walde, D. H. G., & da Rocha, R. P. (2014). Observed summer weather regimes and associated extreme precipitation over Distrito Federal, west-central Brazil. *Environmental Earth Sciences*, *72*(12), 4835–4848. https://doi.org/10.1007/s12665-014-3607-9

Debortoli, S., Dubreuil, N., Funatsu, V., Delahaye, F., de Oliveira, C. H., Rodrigues-Filho, S., et al. (2015). Rainfall patterns in the southern Amazon: A chronological perspective (1971–2010). *Climatic Change*, *132*(2), 251–264. https://doi.org/10.1007/s10584-015-1415-1

Díaz, L. B., Saurral, R., & Vera, C. (2021). Assessment of South America summer rainfall climatology and trends in a set of global climate models large ensembles. *International Journal of Climatology*, *41*(S1), E59–E77. https://doi.org/10.1002/joc.6643

Espinoza, J. C., Arias, P., Moron, V., Junquas, C., Segura, H., Sierra-Pérez, J., et al. (2021). Recent changes in the atmospheric circulation patterns during the dry-to-wet transition season in south tropical South America (1979–2020): Impacts on precipitation and fire season. *Journal of Climate*, *34*, 9025–9042. https://doi.org/10.1175/JCLI-D-21-0303.1

Espinoza, J. C., Garreaud, R., Poveda, G., Arias, P. A., Molina-Carpio, J., Masiokas, M., et al. (2020). Hydroclimate of the Andes part I: Main climatic features. *Frontiers of Earth Science*, *8*, 64. https://doi.org/10.3389/feart.2020.00064

Espinoza, J. C., Lengaigne, M., Ronchail, J., & Janicot, S. (2012). Large-scale circulation patterns and related rainfall in the Amazon basin: A neuronal networks approach. *Climate Dynamics*, *38*(1–2), 121–140. https://doi.org/10.1007/s00382-011-1010-8

Espinoza, J. C., Ronchail, J., Lengaigne, M., Quispe, N., Silva, Y., Bettolli, M. L., et al. (2013). Revisiting wintertime cold air intrusions at the east of the Andes: Propagating features from subtropical Argentina to Peruvian Amazon and relationship with large-scale circulation patterns. *Climate Dynamics*, *41*(7–8), 1983–2002. https://doi.org/10.1007/s00382-012-1639-y

Espinoza, J. C., Ronchail, J., Marengo, J., & Segura, H. (2019). Contrasting north–south changes in Amazon wet-day and dry-day frequency and related atmospheric features (1981–2017). *Climate Dynamics*, *116*(9–10), 5413–5430. https://doi.org/10.1007/s00382-018-4462-2

Eyring, V., Bony, S., Meehl, G. A., Senior, C. A., Stevens, B., Stouffer, R. J., & Taylor, K. E. (2016). Overview of the coupled model Intercomparison project phase 6 (CMIP6) experimental design and organization [Dataset]. Geoscientific Model Development, *9*(5), 1937–1958. https://doi.org/10.5194/gmd-9-1937-2016

Fernández-Granja, J. A., Casanueva, A., Bedia, J., & Fernandez, J. (2021). Improved atmospheric circulation over Europe by the new generation of CMIP6 Earth system models. *Climate Dynamics*, *56*(11–12), 3527–3540. https://doi.org/10.1007/s00382-021-05652-9

Figueroa, M., Armijos, E., Espinoza, J. C., Ronchail, J., & Fraizy, P. (2020). On the relationship between reversal of the river stage (REPIQUETES), rainfall and low-level wind regimes over the Western Amazon basin. *Journal of Hydrology*, *32*, 100752. https://doi.org/10.1016/j.ejrh.2020.100752

Fleig, A. K., Tallaksen, L. M., James, P., Hisdal, H., & Stahl, K. (2015). Attribution of European precipitation and temperature trends to changes in synoptic circulation. *Hydrology and Earth System Sciences*, *19*(7), 3093–3107. https://doi.org/10.5194/hess-19-3093-2015

Fu, R., Yin, L., Li, W., Arias, P. A., Dickinson, R. E., Huang, L., et al. (2013). Increased dry season length over southern Amazonia in recent decades and its implication for future climate projection. *Proceedings of the National Academy of Sciences of the United States of America*, *110*(45), 18110–18115. https://doi.org/10.1073/pnas.1302584110

Funk, C., Peterson, P., Landsfeld, M., Pedreros, D., Verdin, J., Shukla, S., et al. (2014). The climate hazards infrared precipitation with stations—A new environmental record for monitoring extremes. [Dataset]. Scientific Data, *2*:150066. https://doi.org/10.1038/sdata.2015.66

Gan, M. A., Kousky, V. E., & Ropelewski, C. F. (2004). The South America monsoon circulation and its relationship to rainfall over west-central Brazil. *Journal of Climate*, *17*(1), 47–66. https://doi.org/10.1175/1520-0442(2004)017<0047:TSAMCA>2.0.CO;2

Garreaud, R. D. (2009). The Andes climate and weather. *Advances in Geosciences*, *22*, 3–11. https://doi.org/10.5194/adgeo-22-3-2009

Gatti, L. V., Basso, L. S., Miller, J. B., Gloor, M., Gatti Domingues, L., Cassol, H. L., et al. (2021). Amazonia as a carbon source linked to deforestation and climate change. *Nature*, *595*(7867), 388–393. https://doi.org/10.1038/s41586-021-03629-6

Gibson, P. B., Perkins-Kirkpatrick, S. E., & Renwick, J. A. (2016). Projected changes in synoptic weather patterns over New Zealand examined through self-organizing maps. *International Journal of Climatology*, *36*(12), 3934–3948. https://doi.org/10.1002/joc.4604

Giráldez, L., Silva, Y., Zubieta, R., & Sulca, J. (2020). Change of the rainfall seasonality over central Peruvian Andes: Onset, end, duration and its relationship with large-scale atmospheric circulation. *Climate*, *8*(2), 23. https://doi.org/10.3390/cli8020023

Grimm, A. M., Dominguez, F., Cavalcanti, I. F. A., Cavazos, T., Gan, M. A., Silva Dias, P. L., et al. (2020). South and North American monsoons: Characteristics, life cycle, variability, modelling and prediction. In C. P. Chang, K. J. Ha, R. H. Johnson, D. Kim, G. N. C. Lau, & B. Wang (Eds.), *The multi-scale global monsoon system, world scientific series on Asia–Pacific weather and climate* (Vol. 11, pp. 49–66). World Scientific Publishing Company.

Gulizia, C., & Camilloni, I. (2015). Comparative analysis of the ability of a set of CMIP3 and CMIP5 global climate models to represent precipitation in South America. *International Journal of Climatology*, *35*(4), 583–595. https://doi.org/10.1002/joc.4005

Hersbach, H., Bell, B., Berrisford, P., Hirahara, S., Horányi, A., Muñoz-Sabater, J., et al. (2020). The ERA5 global reanalysis. [Dataset]. Quarterly Journal of the Royal Meteorological Society, *146*, 1999–2049. https://doi.org/10.1002/qj.3803

Jones, C., & Carvalho, L. M. V. (2002). Active and break phases in the South American monsoon system. *Journal of Climate*, *15*(8), 905–914. https://doi.org/10.1175/1520-0442(2002)015<0905:aabpit>2.0.co;2

Li, L., & Fu, R. (2006). Influence of cold air intrusions on the wet season onset over Amazonia. *Journal of Climate*, *19*(2), 257–275. https://doi.org/10.1175/jcli3614.1

Llopart, M., Domingues, L. M., Torma, C., Giorgi, F., da Rocha, R. P., Ambrizzi, T., et al. (2020). Assessing changes in the atmospheric water budget as drivers for precipitation change over two CORDEX-CORE domains. *Climate Dynamics*. https://doi.org/10.1007/s00382-020-05539-1

Loikith, P. C., Pampuch, L. A., Slinskey, E., Detzer, J., Mechoso, C. R., & Barkhordarian, A. (2019). A climatology of daily synoptic circulation patterns and associated surface meteorology over southern South America. *Climate Dynamics*, *53*(7–8), 4019–4035. https://doi.org/10.1007/s00382-019-04768-3

Londoño-Arteaga, V., & Lima, C. H. R. (2021). Analysis of CMIP 5 simulations of key climate indices associated with the South America monsoon system. *International Journal of Climatology*, *41*(1), 404–422. https://doi.org/10.1002/joc.6627

Maraun, D., Truhetz, H., & Schaffer, A. (2021). Regional climate model biases, their dependence on synoptic circulation biases and the potential for bias adjustment: A process-oriented evaluation of the Austrian regional climate projections. *Journal of Geophysical Research: Atmospheres*, *126*(6), e2020JD032824. https://doi.org/10.1029/2020jd032824

Marengo, J. A., Liebmann, B., Grimm, A. M., Misra, V., Silva Dias, P. L., Cavalcanti, I. F. A., et al. (2012). Recent developments on the South American monsoon system. *International Journal of Climatology*, *32*, 1–21. https://doi.org/10.1002/joc.2254

Marengo, J. A., Souza, C. M., Jr., Thonicke, K., Burton, C., Halladay, K., Betts, R. A., et al. (2018). Changes in climate and land use over the Amazon region: Current and future variability and trends. *Frontiers of Earth Science*, *6*, 228. https://doi.org/10.3389/feart.2018.00228

Meehl, G. A., Shields, C., Arblaster, J. M., Annamalai, H., & Neale, R. (2020). Intraseasonal, seasonal, and interannual characteristics of regional monsoon simulations in CESM2. *Journal of Advances in Modeling Earth Systems*, *12*(6), e2019MS001962. https://doi.org/10.1029/2019ms001962

Montini, T. L., Jones, C., & Carvalho, L. M. V. (2019). the South American low-level jet: A new climatology, variability, and changes. *Journal of Geophysical Research: Atmospheres*, *124*(3), 1200–1218. https://doi.org/10.1029/2018jd029634

Moron, V., Gouirand, I., & Taylor, M. (2016). Weather types across the Caribbean basin and their relationship with rainfall and sea surface temperature. *Climate Dynamics*, *47*(1–2), 601–621. https://doi.org/10.1007/s00382-015-2858-9

Moron, V., Robertson, A. W., Ward, M. N., & Ndiaye, O. (2008). Weather types and rainfall over Senegal. Part II: Downscaling of GCM simulations. *Journal of Climate*, *21*(2), 288–307. https://doi.org/10.1175/2007jcli1624.1

Nogués-Paegle, J., & Mo, K. (1997). Alternating wet and dry conditions over South America during summer. *Monthly Weather Review*, *125*(2), 279–291. https://doi.org/10.1175/1520-0493(1997)125<0279:awadco>2.0.co;2

Olmo, M., Bettolli, M. L., & Rusticucci, M. (2020). Atmospheric circulation influence on temperature and precipitation individual and compound daily extreme events: Spatial variability and trends over southern South America. *Weather and Climate Extremes*, *29*, 100267. https://doi.org/10.1016/j.wace.2020.100267

Olmo, M. E., & Bettolli, M. L. (2021a). Extreme daily precipitation in southern South America: Statistical characterization and circulation types using observational datasets and regional climate models. *Climate Dynamics*, *57*(3–4), 895–916. https://doi.org/10.1007/s00382-021-05748-2

Olmo, M. E., & Bettolli, M. L. (2021b). Statistical downscaling of daily precipitation over southeastern South America: Assessing the performance in extreme events. *International Journal of Climatology*, *42*(2), 1283–1302. https://doi.org/10.1002/joc.7303

Ortega, G., Arias, P. A., Villegas, J. C., Marquet, P. A., & Nobre, P. (2021). Present-day and future climate over central and South America according to CMIP5/CMIP6 models. *International Journal of Climatology*, *41*(15), 1–23. https://doi.org/10.1002/joc.7221

Pabón-Caicedo, J. D., Arias, P. A., Carril, A. F., Espinoza, J. C., Borrel, L. F., Goubanova, K., et al. (2020). Observed and projected hydroclimate changes in the Andes. *Frontiers of Earth Science*.

Paccini, L., Espinoza, J. C., Ronchail, J., & Segura, H. (2018). Intraseasonal rainfall variability in the Amazon basin related to large-scale circulation patterns: A focus on Western Amazon–Andes transition region. *International Journal of Climatology*, *38*(5), 2386–2399. https://doi.org/10.1002/joc.5341

Parsons, L. A. (2020). Implications of CMIP6 projected drying trends for 21st century Amazonian drought risk. *Earth's Future*, *8*(10), e2020EF001608. https://doi.org/10.1029/2020ef001608

Pascale, S., Carvalho, L. M. V., Adams, D. K., Castro, C. L., & Cavalcanti, I. F. A. (2019). Current and future variations of the monsoons of the Americas in a warming climate. *Current Climate Change Reports*, *5*(3), 125–144. https://doi.org/10.1007/s40641-019-00135-w

Pinto, I., Jack, C., & Hewitson, B. (2018). Process-based model evaluation and projections over southern Africa from coordinated regional climate downscaling experiment and coupled model Intercomparison project phase 5 models. *International Journal of Climatology*, *38*(11), 4251–4261. https://doi.org/10.1002/joc.5666

Quagraine, K. A., Hewitson, B., Jack, C., Wolski, P., Pinto, I., & Lennard, C. (2020). Using co-behaviour analysis to interrogate the performance of CMIP5 GCMs over Southern Africa. *Journal of Climate*, *33*(7), 2891–2905. https://doi.org/10.1175/jcli-d-19-0472.1

Reboita, M. S., Kuki, C. A. C., Marrafon, V. H., de Souza, C. A., Ferreira, G. W. S., Teodoro, T., & Lima, J. W. M. (2021). South America climate change revealed through climate indices projected by GCMs and Eta-RCM ensembles. *Climate Dynamics*, *58*(1–2), 459–485. https://doi.org/10.1007/s00382-021-05918-2

Reis, S. M., Marimon, B. S., Marimon, B. H., Morandi, P. S., Almeida de Oliveira, E., Elias, F., et al. (2018). Climate and fragmentation affect forest structure at the southern border of Amazonia. *Plant Ecology & Diversity*, *11*(1), 13–25. https://doi.org/10.1080/17550874.2018.1455230

Ruiz-Vásquez, M., Arias, P. A., Martínez, J. A., & Espinoza, J. C. (2020). Effects of Amazon basin deforestation on regional atmospheric circulation and water vapor transport towards tropical South America. *Climate Dynamics*, *54*(9–10), 4169–4189. https://doi.org/10.1007/s00382-020-05223-4

Sakaguchi, K., Leung, L. R., Burleyson, C. D., Xiao, H., & Wan, H. (2018). Role of troposphere-convection-land coupling in the south-Western Amazon precipitation bias of the community Earth system model version 1 (CESM1). *Journal of Geophysical Research: Atmospheres*, *123*(16), 8374–8399. https://doi.org/10.1029/2018jd028999

San Martín, D., Manzanas, R., Brands, S., Herrera, S., & Gutiérrez, J. M. (2017). Reassessing model uncertainty for regional projections of precipitation with an ensemble of statistical downscaling methods. *Journal of Climate*, *30*(1), 203–223. https://doi.org/10.1175/jcli-d-16-0366.1

Schuenemann, K. C., & Cassano, J. J. (2009). Changes in synoptic weather patterns and Greenland precipitation in the 20th and 21st centuries: 1. Evaluation of late 20th century simulations from IPCC models. *Journal of Geophysical Research*, *114*(D20), D20113. https://doi.org/10.1029/2009JD011705

Segura, H., Junquas, C., Espinoza, J. C., Vuille, M., Jauregui, Y. R., Rabatel, A., et al. (2019). New insights into the rainfall variability in the tropical Andes on seasonal and interannual time scales. *Climate Dynamics*, *53*(1–2), 405–426. https://doi.org/10.1007/s00382-018-4590-8

Sena, A., & Magnusdottir, G. (2020). Projected end-of-century changes in the South American monsoon in the CESM large ensemble. *Journal of Climate*, *33*(18), 7859–7874. https://doi.org/10.1175/jcli-d-19-0645.1

Sierra, J. P., Arias, P. A., & Vieira, S. C. (2015). Precipitation over northern South America and its seasonal variability as simulated by the CMIP5 models. *Advances in Meteorology*, *2015*, 1–22. https://doi.org/10.1155/2015/634720

Sierra, J. P., Junquas, C., Espinoza, J. C., Segura, H., Condom, T., Andrade, M., et al. (2021). Deforestation impacts on Amazon-Andes hydroclimatic connectivity. *Climate Dynamics*, *58*(9–10), 2609–2636. https://doi.org/10.1007/s00382-021-06025-y

Silva, C. H. L., Jr., Aragão, L. E. O. C., Anderson, L. O., Fonseca, M. G., Shimabukuro, Y. E., Vancutsem, C., et al. (2020). Persistent collapse of biomass in Amazonian forest edges following deforestation leads to unaccounted carbon losses. *Science Advances*, *6*(40), eaaz8360. https://doi.org/10.1126/sciadv.aaz8360

Solman, S. A. (2013). Regional climate modeling over South America: A review. *Advances in Meteorology*, *2013*, 504357. https://doi.org/10.1155/2013/504357

Staal, A., Tuinenburg, O., Bosmans, J., Dekker, S. C., van Nes, E. H., Scheffer, M., et al. (2018). Forest-rainfall cascades buffer against drought across the Amazon. *Nature Climate Change*, *8*(6), 539–543. https://doi.org/10.1038/s41558-018-0177-y

Stryhal, J., & Huth, R. (2018). Classifications of winter atmospheric circulation patterns: Validation of CMIP5 GCMs over Europe and the North Atlantic. *Climate Dynamics*, *52*(5–6), 3575–3598. https://doi.org/10.1007/s00382-018-4344-7

Taylor, K. E. (2001). Summarizing multiple aspects of model performance in a single diagram. *Journal of Geophysical Research*, *106*(D7), 7183–7192. https://doi.org/10.1029/2000jd900719

Teodoro, T. A., Reboita, M. S., Llopart, M., da Rocha, R. P., & Ashfaq, M. (2021). Climate change impacts on the South American monsoon system and its surface–atmosphere processes through RegCM4 CORDEX-CORE projections. *Earth Systems and Environment*, *5*(4), 825–847. https://doi.org/10.1007/s41748-021-00265-y

Thaler, V., Loikith, P. C., Mechoso, C. R., & Pampuch, L. A. (2021). A multivariate assessment of climate change projections over South America using the fifth phase of the Coupled Model Intercomparison Project. *International Journal of Climatology*, *41*(8), 4265–4282. https://doi.org/10.1002/joc.7072

Vera, C., Higgins, W., Amador, J., Ambrizzi, T., Garreaud, R., Gochis, D., et al. (2006). Toward a unified view of the American monsoon systems. *Journal of Climate*, *19*(20), 4977–5000. https://doi.org/10.1175/jcli3896.1

Wainwright, C. M., Black, E., & Allan, R. P. (2021). Future changes in wet and dry season characteristics in CMIP5 and CMIP6 simulations. *Journal of Hydrometeorology*, *22*(9), 2339–2357. https://doi.org/10.1175/jhm-d-21-0017.1

Wang, B., Zheng, L., Liu, D. L., Ji, F., Clark, A., & Yu, Q. (2018). Using multi-model ensembles of CMIP5 global climate models to reproduce observed monthly rainfall and temperature with machine learning methods in Australia. *International Journal of Climatology*, *38*(13), 4891–4902. https://doi.org/10.1002/joc.5705

Wang, H., & Fu, R. (2002). Cross-equatorial flow and seasonal cycle of precipitation over South America. *Journal of Climate*, *15*(13), 1591–1608. https://doi.org/10.1175/1520-0442(2002)015<1591:cefasc>2.0.co;2

Wang, H., & Fu, R. (2004). Influence of cross-Andes flow on the South American low-level jet. *Journal of Climate*, *17*(6), 1247–1262. https://doi.org/10.1175/1520-0442(2004)017<1247:iocfot>2.0.co;2

Wilks, D. S. (2019). *Statistical methods in the atmospheric sciences* (4th ed., p. 840). Elsevier.

Wongchuig, S., Espinoza, J. C., Condom, T., Segura, H., Ronchail, J., Arias, P. A., et al. (2021). A regional view of the linkages between hydro-climatic changes and deforestation in the Southern Amazon. *International Journal of Climatology*, 1–19. Accepted Author Manuscript. https://doi.org/10.1002/joc.7443

Yin, L., Fu, R., Shevliakova, E., & Dickinson, R. E. (2013). How well can CMIP5 simulate precipitation and its controlling processes over tropical South America? *Climate Dynamics*, *41*(11–12), 3127–3143. https://doi.org/10.1007/s00382-012-1582-y

Yin, L., Fu, R., Zhang, Y., Arias, P. A., Fernando, N., Li, W., et al. (2014). What controls interannual variations of the wet season onsets over the Amazon? *Journal of Geophysical Research: Atmospheres*, *119*(5), 2314–2328. https://doi.org/10.1002/2013jd021349

Zhang, K., de Castanho, A. D. A., Galbraith, D. R., Moghim, S., Levine, N. M., Bras, R. L., et al. (2015). The fate of Amazonian ecosystems over the coming century arising from changes in climate, atmospheric CO2, and land use. *Global Change Biology*, *21*(7), 2569–2587. https://doi.org/10.1111/gcb.12903

Zilli, M. T., & Carvalho, L. M. V. (2021). Detection and attribution of precipitation trends associated with the poleward shift of the South Atlantic Convergence Zone using CMIP5 simulations. *International Journal of Climatology*, *41*(5), 3085–3106. https://doi.org/10.1002/joc.7007

References From the Supporting Information

Bentsen, M., Bethke, I., Debernard, J. B., Iversen, T., Kirkevåg, A., Seland, Ø., et al. (2013). The Norwegian Earth system model, NORESM1-M - Part 1: Description and basic evaluation of the physical climate. *Geoscientific Model Development*, *6*(3), 687–720. https://doi.org/10.5194/gmd-6-687-2013

Boucher, O., Servonnat, J., Albright, A. L., Aumont, O., Balkanski, Y., Bastrikov, V., et al. (2020). Presentation and evaluation of the IPSL-CM6A-LR climate model. *Journal of Advances in Modeling Earth Systems*, *12*, e2019MS002010.

Danabasoglu, G. (2019). *NCAR CESM2 model output prepared for CMIP6 CMIP historical*. Earth System Grid Federation. https://doi.org/10.22033/ESGF/CMIP6.7627

Döscher, R., Acosta, M., Alessandri, A., Anthoni, P., Arneth, A., Arsouze, T., et al. (2021). The EC-Earth3 Earth system model for the climate model Intercomparison project 6. *Geoscientific Model Development Discussions*, *15*(7), 2973–3020. https://doi.org/10.5194/gmd-2020-446

Fogli, P. G., Iovino, D., & Lovato, T. (2020). CMCC CMCC-CM2-SR5 model output prepared for CMIP6 OMIP *OMIP1. Earth System Grid Federation*.

Held, I. M., Guo, H., Adcroft, A., Dunne, J. P., Horowitz, L. W., Krasting, J., et al. (2019). Structure and performance of GFDL's CM4.0 climate model. *Journal of Advances in Modeling Earth Systems*, *11*, 3691–3727. https://doi.org/10.1029/2019MS001829

Li, L., Yu, Y., Tang, Y., Lin, P., Xie, J., Song, M., et al. (2020). The flexible global ocean-atmosphere-land system model grid-point version 3 (FGOALS-g3): Description and evaluation. *Journal of Advances in Modeling Earth Systems*, *12*(9), e2019MS002012. https://doi.org/10.1029/2019ms002012

Mueller, W. A., Jungclaus, J. H., Mauritsen, T., Baehr, J., Bittner, M., Budich, R., et al. (2018). A high-resolution version of the max planck institute Earth system model MPI-ESM1.2-HR. *Journal of Advances in Modeling Earth Systems*, *10*, 1383–1413.

Scoccimarro, E., Bellucci, A., & Peano, D. (2019). CMCC CMCC-CM2-HR4 model output prepared for CMIP6 HighResMIP hist-195*0. Earth System Grid Federation*.

Swart, N. C., Cole, J. N. S., Kharin, V. V., Lazare, M., Scinocca, J. F., Gillett, N. P., et al. (2019). The Canadian Earth system model version 5 (CanESM5.0.3). *Geoscientific Model Development Discussions*, *5*(11), 1–68. https://doi.org/10.5194/gmd-2019-177

Tatebe, H., Ogura, T., Nitta, T., Komuro, Y., Ogochi, K., Takemura, T., et al. (2019). Description and basic evaluation of simulated mean state, internal variability, and climate sensitivity in MIROC6. *Geoscientific Model Development*, *12*(7), 2727–2765. https://doi.org/10.5194/gmd-12-2727-2019

Wu, T., Yu, R., Lu, Y., Jie, W., Fang, Y., Zhang, J., et al. (2021). BCC-CSM2-HR: A high-resolution version of the Beijing climate center climate system model. *Geoscientific Model Development*, *14*(5), 2977–3006. https://doi.org/10.5194/gmd-14-2977-2021

Wu, T., Zhang, F., Zhang, J., Jie, W., Zhang, Y., Wu, F., et al. (2020). Beijing climate center Earth system model version 1 (BCC-ESM1): Model description and evaluation of aerosol simulations. *Geoscientific Model Development*, *13*(3), 977–1005. https://doi.org/10.5194/gmd-13-977-2020

Ziehn, T., Chamberlain, M. A., Law, R., Lenton, A., Bodman, R. W., Dix, M., et al. (2020). The Australian Earth system model: ACCESS-ESM1.5. *Journal of Southern Hemisphere Earth Systems Science*, *70*(1), 193. https://doi.org/10.1071/es19035